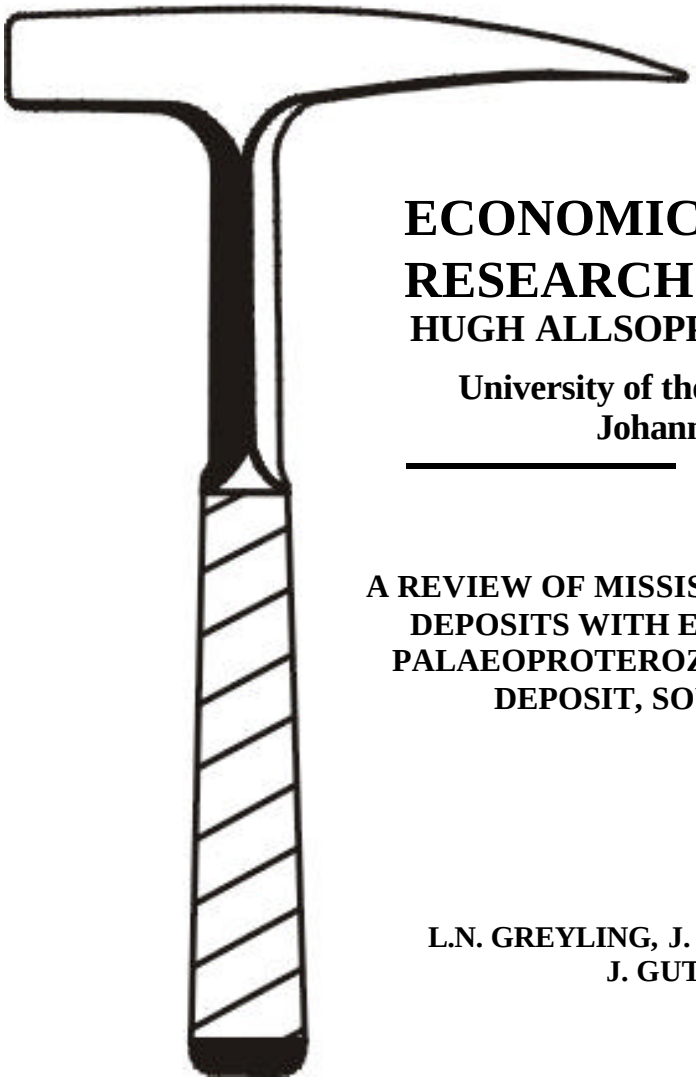

ECONOMIC GEOLOGY RESEARCH INSTITUTE

HUGH ALLSOPP LABORATORY

University of the Witwatersrand
Johannesburg

A REVIEW OF MISSISSIPPI VALLEY-TYPE DEPOSITS WITH EMPHASIS ON THE PALAEOPROTEROZOIC PERING Pb-Zn DEPOSIT, SOUTH AFRICA

L.N. GREYLING, J. M. HUIZENGA and J. GUTZMER

INFORMATION CIRCULAR No. 356

UNIVERSITY OF THE WITWATERSRAND

JOHANNESBURG

A REVIEW OF MISSISSIPPI VALLEY-TYPE DEPOSITS WITH EMPHASIS ON THE PALAEOPROTEROZOIC PERING Pb-Zn DEPOSIT, SOUTH AFRICA

by

L.N. GREYLING[1,2], J. M. HUIZENGA[1] and J. GUTZMER[1]

([1]Department of Geology, Rand Afrikaans University, P.O. Box 524, Auckland Park 2006, South Africa;
[2] Present address: Economic Geology Research Institute, School of Geosciences, University of the Witwatersrand, Private Bag 3, WITS, 2050, South Africa)

ECONOMIC GEOLOGY RESEARCH INSTITUTE
INFORMATION CIRCULAR No. 356

December, 2001

A REVIEW OF MISSISSIPPI VALLEY-TYPE DEPOSITS WITH EMPHASIS ON THE PALAEOPROTEROZOIC PERING Pb-Zn DEPOSIT, SOUTH AFRICA

ABSTRACT

Mississippi Valley-type deposits are epigenetic Pb-Zn deposits generally hosted in platform carbonate successions of Phanerozoic age. Hydrothermal fluid components include metal-bearing brines (consisting of ~10-30 wt.% salts at temperatures between 75 and 200 °C) and sulphur-bearing fluids. Metals are generally transported as chloride-, and reduced-sulphur complexes in aqueous solutions. Sulphide mineralisation is a result of fluid migration and focussing. Mechanisms for the precipitation of MVT deposits include sulphur addition, sulphate reduction, and the destabilisation of organic complexes.

The Pering deposit in the Northwest Province, South Africa, is hosted by the Palaeoproterozoic stromatolitic dolomites of the Transvaal Supergroup, and although direct dating the mineralisation has not yet been successful, it is also constrained as Palaeoproterozoic in age. It has been classified as a Mississippi Valley-type deposit based on its mineralogy, geological setting, and mineral chemistry, and is, together with the Bushy Park Pb-Zn deposit and the F-Pb-Zn deposits near Zeerust, the only known MVT deposit of Palaeoproterozoic age. The Pering open cast mine has been operational since 1986, yielding 18 Mt at an average ore grade of 3.6 wt.% Zn and 0.6 wt.% Pb. Excellent exposures in the open pit, and closely spaced diamond drill core enables the detailed study of this unique deposit.

The mineralogy includes sphalerite, galena and minor chalcopyrite as ore minerals, with diagenetic pyrite, hydrothermal dolomite, quartz and calcite as gangue minerals. Sphalerite predominates over galena. Mineralisation occurs as: (1) disseminated stratabound replacement sheets restricted mainly to stromatolitic zones of the Steekdorings Member of the Reivilo Formation; and (2) open space infill in breccia bodies that cross cut the stratigraphy. Three events of hydrothermal brecciation, resultant from prolonged pulses of fluid infiltration, and mineralisation are recognised. The first brecciation event is marked by the cementation of the dolomite host rock by sparry dolomite, closely associated with fine-grained disseminated sphalerite and galena. The second brecciation event is of minor importance, and is marked by the formation of small amounts of the second sphalerite generation, while the third, and final, brecciation event is marked by the formation of euhedral sphalerite, galena, quartz, sparry dolomite, and calcite as open space fill.

_____oOo_____

A REVIEW OF MISSISSIPPI VALLEY-TYPE DEPOSITS WITH EMPHASIS ON THE PALAEOPROTEROZOIC PERING Pb-Zn DEPOSIT, SOUTH AFRICA

CONTENTS

oOo

Published by the Economic Geology Research Institute
(incorporating the Hugh Allsopp Laboratory)
School of Geosciences
University of the Witwatersrand
1 Jan Smuts Avenue
Johannesburg
South Africa

http://www.wits.ac.za/egru/research.htm

ISBN 1-86838-299-0

A REVIEW OF MISSISSIPPI VALLEY-TYPE DEPOSITS WITH EMPHASIS ON THE PALAEOPROTEROZOIC PERING Pb-Zn DEPOSIT, SOUTH AFRICA

INTRODUCTION

The Mississippi Valley in the southeastern United States of America is the type locality for this very distinctive type of carbonate-hosted Pb-Zn deposits, where flat to gentle dips prevail and large Mississippi Valley-type (MVT) deposits occur in several districts (Guilbert and Park, 1986). MVT deposits are typically stratabound, epigenetic, base-metal deposits that primarily occur in dolomite, rarely in limestone or sandstone (Sverjenski, 1986), and are generally Phanerozoic in age (Fig. 1a) (Leach and Sangster, 1993). Individual ore bodies are generally small and yield less than 10 Mt of ore (grades seldom exceed 10% Pb+Zn) (Fig. 1b), but usually occur in clusters or groups of deposits (Leach and Sangster, 1993). Zinc is generally the dominant ore constituent (Fig. 1c), except in the lead-rich southeast Missouri district (Sverjenski, 1986).

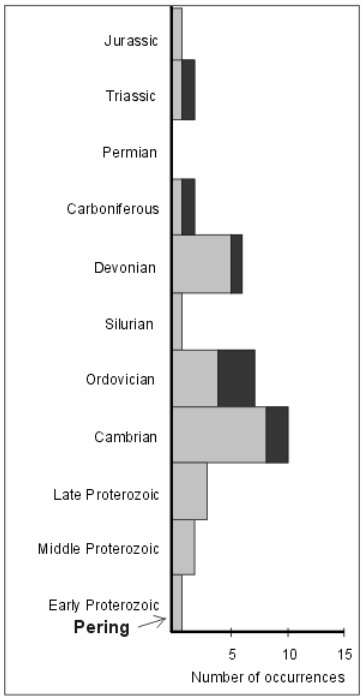

Figure 1a The distribution of MVT-deposits as a function of age. Light grey areas are MVT deposits, and dark grey areas indicate MVT districts (modified from Leach & Sangster, 1993). The Pering deposit is indicated as an Early Proterozoic occurrence.

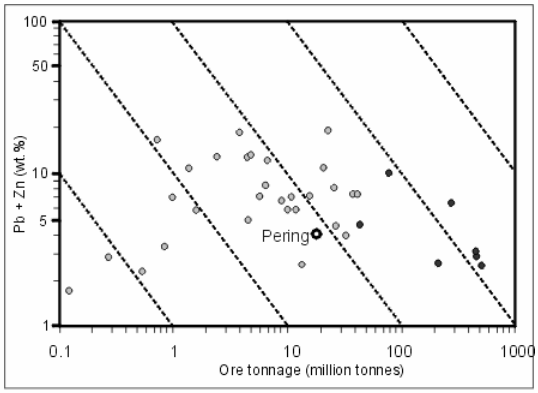

Figure 1b MVT deposits presented according to the estimated ore tonnage in Mt and Pb+Zn wt.%. The Pering deposit plots at 18 Mt and Pb+Zn of 4.2 wt.%, as estimated by Wheatley et al. (1986). Dark grey spheres indicate MVT districts, whereas light grey spheres denote individual MVT deposits (after Leach & Sangster, 1993).

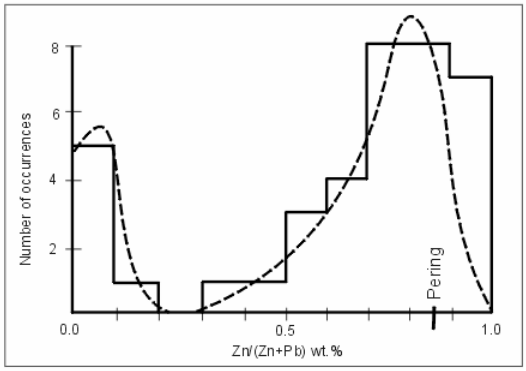

Figure 1c Distribution of MVT-deposits as a function of Zn/(Zn+Pb) in wt.% (from Leach & Sangster, 1993).

The Palaeoproterozoic Pering deposit is located in the dolomites of the Transvaal Supergroup in the Northwest Province, South Africa. It is considered as one of the oldest MVT deposits worldwide. The Pering deposit, in contrast to most other Pb-Zn occurrences in the Transvaal dolomites, provides excellent mining-related exposure with tightly spaced diamond drill core and open-pit mining methods. This offers ample opportunity to study the character of mineralization in great detail.

This paper reviews some of the fundamentals of MVT ore-forming solutions, with subsequent emphasis on the geological setting and mineralogy of the Pering Pb-Zn deposit.

GEOLOGICAL SETTING AND STRUCTURE OF MVT DEPOSITS

Carbonate successions in areas of shallow crustal depths in structurally passive regions along basin margins are the favourite depositional environments for MVT deposits. Classical papers on MVT deposits by Ohle (1959, 1980) characterise these deposits according to their tendency to occur along lines of facies change, i.e., reef to off-reef, shelf dolomite to basin limestone, or carbonate to shale. The formation of MVT deposits shows no relation to igneous activity (Guilbert and Park, 1986; Sverjenski, 1986; Leach and Sangster, 1993). MVT deposits form when dense, metalliferous basinal brines (10-30 wt.% salts) at 75 °C to 200 °C (Leach and Sangster, 1993) migrate updip from shale basins into relatively undeformed platform-carbonate sequences along basin margins (Guilbert and Park, 1986). These fluids are products of regional or sub-continental scale hydrological processes (Leach and Sangster, 1993). The mobilisation and migration of hydrothermal fluids and subsequent ore deposition are attributed to such processes as diagenetic compaction of shales, seismic pumping or gravitative flow, and flow along regional groundwater aquifers that provided subtle permeability. Mineral deposition may take place along suitable structures, such as breccias, facies tracts, faults and basement highs that permit the upward migration and escape of the hydrothermal fluids from the aquifer (Sverjenski, 1986). MVT deposits are, therefore, usually laterally extensive (districts usually cover several hundreds of square kilometres), but relatively thin in vertical dimension (<100 m vertical thickness), suggesting that the horizontal component of mineralising fluid movement far exceeded the vertical component (Guilbert and Park, 1986).

Ores often appear as stratabound replacement sheets in dolomite, or dolomitized limestone. Mineralisation also occurs as: (1) open-space infill in solution-collapse breccias; (2) in veins; and (3) in fold-related joints and fractures in carbonate rocks (e.g., Leach and Sangster, 1993).

MINERALOGY

The mineralogy of MVT deposits is typically simple, dominated by low-silver galena, low-iron sphalerite, barite, and fluorite. Coating of sphalerite crystals with oil or asphaltic, kerogen-rich compounds were found in the Tri-State region in the United States of America, which indicates the presence of hydrocarbons as an integral component of the mineralising system (Leach and Sangster, 1993). Gangue minerals include dolomite, calcite, and minor chert/chalcedony or jasper, and quartz. Pyrite and marcasite, as well as some chalcopyrite, may be present in minor amounts. The geochemistry of MVT deposits is marked by the presence of notable concentrations of minor[1] and trace[2] elements (for example Fe, Co, Ni, Cd), indicating that the ore solutions had sufficient capacity to transport considerable concentrations of metal ions.

In virtually all MVT districts dolomitisation of the host rock around the deposits is evident. This dolomitisation may be either of hydrothermal or diagenetic nature (Guilbert and Park, 1986). In the former case economic mineral concentrations may be distinctly rimmed by halos of dolomite. These halos may vary from a few centimetres to several kilometres wide. Silicification, pyritisation and recrystallisation are other common effects of hydrothermal wall-rock alteration around MVT deposits. Recrystallisation and wall-rock alteration effects normally occur along zones of mineralised breccias and affect dolomite that has replaced the primary limestone.

[1] Minor elements: 0.1-1.0 oxide wt.% (Rollinson, 1993).
[2] Trace elements: < 0.1 oxide wt.% expressed in ppm (Rollinson, 1993).

GEOCHEMISTRY

Hydrothermal fluids are, by definition, hot, multi-component electrolyte solutions, with the most important solutes being alkali chlorides ($NaCl \pm KCl \pm CaCl_2 \pm MgCl_2$) with salinities ranging from dilute to very saline brines (NaCl equivalent in excess of 50 wt.%) (Roedder, 1984). A hydrothermal solution reacts with the crustal rocks it moves through, and therefore changes continuously in composition. These changes may enable the hydrothermal solution to extract certain metals from surrounding host rocks, to transport these metals in solution, and subsequently precipitate them in high concentrations at certain localities. Ore metals such as lead, zinc, molybdenum, tin and silver constitute less than 0.01% of the crust. Lead occurs primarily in alkali feldspars, whereas zinc, copper, and tin are leached from clays, micas, pyroxenes and amphiboles (Skinner, 1997).

A major constraint on the formation of epigenetic hydrothermal lead-zinc deposits is the low solubility of lead and zinc sulphide in aqueous solutions (Fig. 2). Thus, only small quantities of lead and zinc can be transported in a reduced sulphide solution, and unrealistically large volumes of such a fluid are required to form economic lead-zinc deposits (Sverjensky, 1981). It is generally assumed that solutions carrying at least 10 ppm Zn and 10 ppm Pb are required to form an average MVT deposit (Barnes, 1979; Giordano and Barnes, 1979).

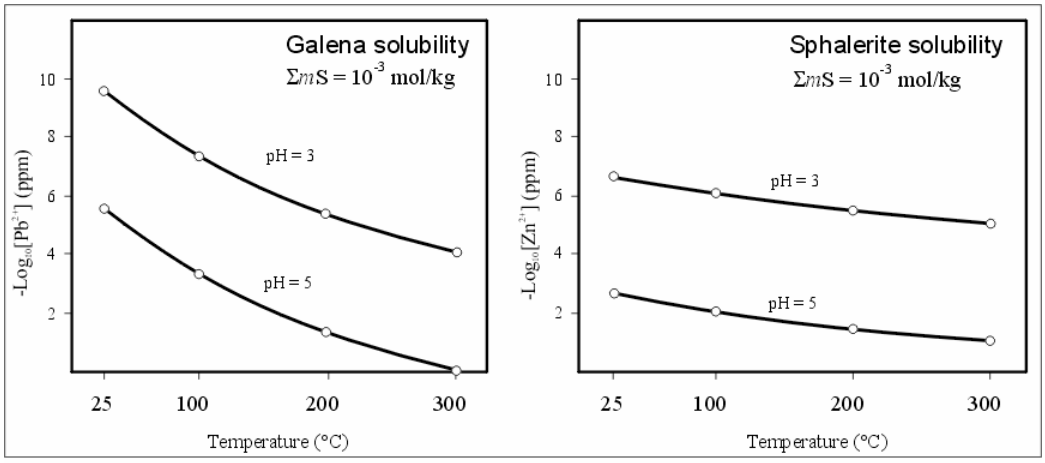

Figure 2 Variation in solubilities of galena and sphalerite in an aqueous solution defined as a function of pH and temperature. Experimental results are presented as data points affixed by lines (data from Wood & Samson, 1998).

Fluid inclusion studies and stable isotope (C, O, H, S) geochemistry are the most widely used techniques in characterising the pressure-temperature-composition conditions of hydrothermal mineral deposits, with the aim of establishing the mechanism of ore formation, and the source of metals and sulphur. The general physico-chemistry of a typical hydrothermal fluid responsible for the formation of a MVT lead-zinc system is listed in Table 1 (Giordano and Barnes, 1981). The temperature of mineralisation for MVT deposits varies between 100 °C and 200 °C. MVT deposits are thought to form at shallow crustal levels (<1 km), although an exact pressure of mineralisation can generally not be determined with accuracy. Typically, hydrothermal solutions show an increasing oxygen fugacity ($\log_{10} fO_2$) of -54 to -41 for increasing temperatures between 100 °C and 200 °C, a near neutral pH ($pH_{neutral} \pm 1$), and contain small amounts of CO_2. The average salinity is 20-30 wt.% NaCl equivalent (i.e., 4.2-6.7 mol/kg).

Table 1: General characteristics of an MVT-deposit-forming hydrothermal solution, with an average salinity of 20-30 wt.% NaCl equiv. (4.2 – 6.7 mol/kg) (modified after Giordano and Barnes, 1981; Seward and Barnes, 1997)

	100 °C	200 °C
ΣmS	10^{-1} to 10^{-3} mol/kg	10^{-1} to 10^{-3} mol/kg
ΣmC	10^{-2} to 10^{-4} mol/kg	10^{-2} to 10^{-4} mol/kg
$\log_{10} fO_2$	-54 to –58	-41 to –46
pH	5.1 to 7.1	4.7 to 6.7
$pH_{neutral}$	6.1	5.7

Solubility of lead and zinc in aqueous solutions

Lead and zinc are borderline acids, according to Pearson's classification (1963) and occur in the divalent oxidation state. Both these metals behave in similar fashions in solutions, with Pb^{2+} being softer than Zn^{2+} (Pearson, 1963). In order to transport lead and zinc sulphides in an aqueous solution, complexation is needed to increase the solubility of these metals (e.g., Wood and Samson, 1998). Complex ions are formed between metals and ligands[3] in solution and act as carriers of metals. The activities of these ligands determine the ore-carrying capacity of the hydrothermal fluid. The activity of a ligand is, in turn, determined by several factors including the concentration, temperature, ionic strength, extent of ion pairing with aqueous species, pH, and fO_2 of the solution (Barnes, 1979). This section provides a brief overview of important mechanisms of lead-zinc complexation in hydrothermal solutions. For a more detailed discussion, the reader is referred to Wood and Samson (1998) and the references therein.

Chloride and sulphur complexation

The most important inorganic complex ions to consider for transportation of metals in hydrothermal solutions (Barnes, 1979) are:

(1) chloride complexes (e.g., $ZnCl_n^{(2-n)}$ and $PbCl_n^{(2-n)}$, n = 1, 2, 3, 4); and

(2) reduced sulphur complexes (e.g., $Zn(HS)_n^{(2-n)}$, where n = 2, 3, 4, and $Pb(HS)_n^{(2-n)}$, where n = 2, 3).

Other complexes are possible (e.g., with Br^-, $(CN)^-$), but are not realistic because of the usually low concentrations of the respective ligands in hydrothermal solutions. Significant amounts of lead (>10 ppm) can only be dissolved at high temperatures (≥200 °C) and at either low pH (<3) or high fO_2 ($\log_{10} fO_2 \geq -40$) as seen in Figure 3. Reduced sulphur complexes become significant ligands at very high concentrations of total sulphur in the fluid ($\Sigma mS > 10^{-2}$ mol/kg) as shown in Figure 4. Concentrations of 10 ppm Pb and Zn in hydrothermal fluids can only be reached by sulphur complexation at a total sulphur content of 1 mol/kg. As seen from Table 1 such concentrations are highly unlikely in natural systems (Giordano and Barnes, 1981).

[3] The most important ligands in hydrothermal solutions are Cl^-, HS^-, OH^- and CH_3COO^-. Other ligands include NH_3, F^-, Br^-, I^-, $(S_2O_3)^{2-}$, $(HSO_4)^-$, $(SO_4)^{2-}$, $(HCO_3)^-$, $(CO_3)^{2-}$.

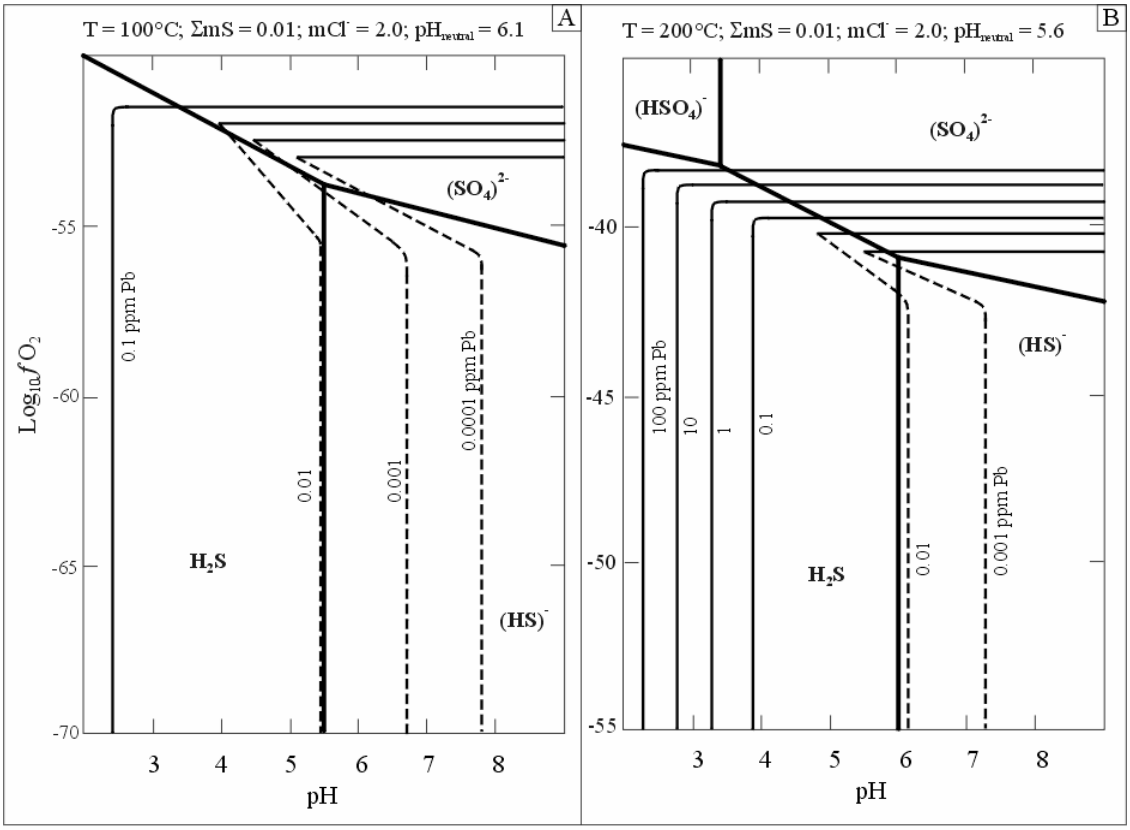

Figure 3 LogfO_2-pH diagram for the system H-S-O at 100 °C (A) and 200 °C (B). The diagrams show the solubility of Pb (ppm) in sulphur complexes (dashed lines) and chloride complexes (solid lines). Thick solid lines separate the various fields of the sulphur species. The Pb solubility increases with increasing temperature, and/or decreasing pH, and/or increasing fO_2. Figure modified after Barnes (1979). See text for further discussion.

Increasing chloride concentrations from 1 mol/kg to 5 mol/kg increases the solubility of lead and zinc by a factor of 100 at temperatures below 100 °C (Fig. 5). As seen in Figure 5, the effect of increasing salinity on the solubility of lead and zinc becomes smaller at higher temperatures. The solubility of galena in chloride solutions is a factor 10-1000 smaller than that of sphalerite. It follows that lead-zinc-chloride complexes should dominate in hydrothermal solutions. Sulphide complexes can only be present in significant amounts at extremely high sulphide concentrations. Sulphide complexes, therefore, only play a limited role in the transportation of Pb and Zn in hydrothermal solutions. In order to form a hydrothermal mineralising chloride solution, high temperatures (> 200 °C) and either a low pH (< 3) or a high fO_2 ($\approx 10^{-40}$ bar) are required. Such conditions (specifically pH and fO_2) are not typically encountered in fluid inclusions in ore and gangue minerals from MVT deposits. Mineralising fluids typically have salinities of 20-30 wt.% NaCl equivalent (m_{NaCl} = 4.2 - 6.7 mol/kg) (Sicree and Barnes, 1996). Chloride complexation alone would not suffice to carry large concentrations of lead and zinc in solution. Therefore, other ligands must play an additional role in the precipitation of lead and zinc from hydrothermal solutions. The most likely alternative ligands to consider for lead-zinc complexation are oxidised sulphur and hydrocarbons from an organic source.

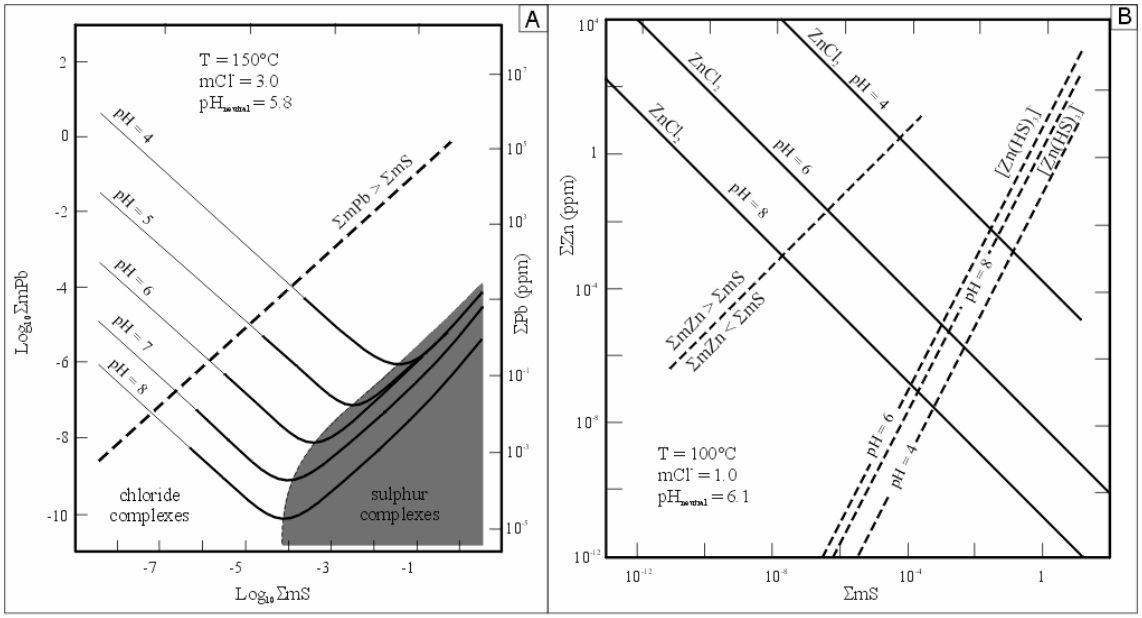

Figure 4 Pb and Zn solubility vs. total sulphur content as a function of pH. Diagram (A) is constructed for Pb solubility at 150 °C. Diagram (B) demonstrates Zn solubility at 100 °C. The figures show the dominant areas of sulphur and chloride complexation (after Giordano & Barnes, 1979).

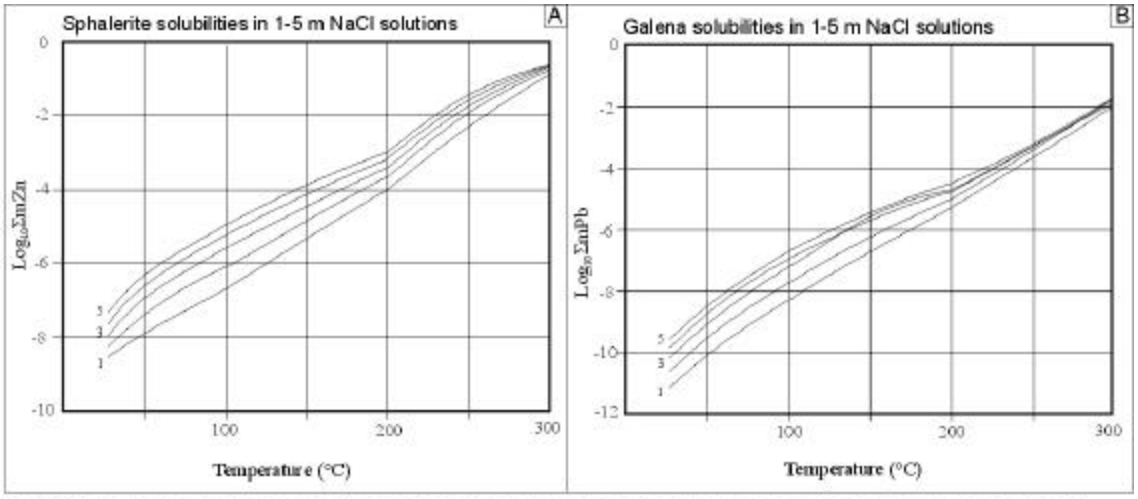

Figure 5 Solubilities for sphalerite (diagram A) and galena (diagram B) in 1-5 m NaCl solutions as a function of temperature. A clear trend is visible indicating increasing solubility of both ZnS and PbS with increasing NaCl (modified after Barrett & Anderson, 1988).

Oxidised sulphur complexation

The solubility of lead and zinc is efficiently increased by oxidised and partly oxidised sulphur ligands such as sulphate ($(SO_4)^{2-}$) or thio-sulphate ($(S_2O_3)^{2-}$). Such complexes require solutions with relatively high fO_2 ($\log_{10} fO_2 > -55$ at 100 °C and $\log_{10} fO_2 > -48$ at 200 °C) and near neutral pH conditions (see Fig. 5), very similar to those observed in typical MVT deposits. The simultaneous transport of metal and oxidised sulphur in one fluid is an additional distinctive advantage of this complexation mechanism (Anderson, 1991) as it renders the presence of a second hydrothermal fluid unnecessary.

Organic complexation

The presence of organic material (e.g., bitumen, oil, kerogen and graphite), in many MVT districts have led Sicree and Barnes (1996) to suggest that organic lead-zinc complexation may have played a major role in metal transport. Sicree and Barnes (1996) have carried out a

number of solubility experiments using solutions with organic ligands, but were unable to identify a suitable organic ligand able to transport significant amounts of lead and zinc in organic complexes. While the possibility of transporting lead and zinc in organic complexes cannot be disregarded at this stage, more research needs to be done on this subject (Sicree and Barnes, 1996).

MODELS FOR MVT Pb-Zn MINERALISATION

Several models exist to explain the formation MVT lead-zinc deposits. This section reviews the most important models using the publications of Spirakis and Heyl (1995) and Sicree and Barnes (1996). Models explaining mineral precipitation can be summarised as follows (Sicree and Barnes, 1996):

Sulphur addition

Lead and zinc are transported in an aqueous basinal brine fluid as chloride complexes. Addition of sulphur results in the following irreversible precipitation reaction (Barnes, 1979):

$$PbCl_{2(aq)} + H_2S_{(aq)} \rightarrow PbS_{(s)} + 2H^+ + 2Cl^-$$

Sulphur is made available from:

(1) a second fluid. Precipitation occurs at the site of mixing;
(2) sulphide, which is released from thermally degrading organic material at the site of mineralisation. A significant amount of organic material must be present to supply the necessary H_2S; and
(3) reduction of sulphate of evaporite minerals (i.e., gypsum and barite). The reducing agent may be organic material (of which large amounts are required) or methane liberated from organic material at temperatures higher than 150 °C. Relatively small amounts of organic material are needed at these temperatures to efficiently generate sulphide sulphur (Anderson, 1991).

Sulphate reduction

Lead and zinc are transported in one sulphate-chloride-bearing brine. Precipitation occurs by reduction of sulphate to sulphide by methane and/or organic material:

(1) methane derived from organic material. The following irreversible reaction will occur:

$$CH_4 + 2H^+ + (SO_4)^{2-} \rightarrow H_2S + CO_2 + 2H_2O$$

The H_2S produced by this reaction is used for PbS and ZnS precipitation;

(2) organic material (either CH_2O or CH_2) present at the mineralisation site or in the fluid. Thermochemical sulphate reduction occurs as follows (Orr, 1974, 1982):

$$2H^+ + (SO_4)^{2-} + 3H_2S \rightarrow 4S^0 + 4H_2O \quad (2.1)$$

and subsequently:

$$(CH_2O) + 2S^0 + H_2O \rightarrow CO_2 + 2H_2S \quad (2.2a)$$

Reaction (1) and (2a): $2H^+ + 2(CH_2O) + (SO_4)^{2-} \rightarrow H_2S + 2H_2O + 2CO_2$ (2.2b)

or:

$$4(CH_2) + 12S^0 + 8H_2O \rightarrow 12H_2S + 4CO_2 \quad (2.3a)$$

Reaction (1) and (3a): $6H^+ + 3(SO_4)^{2-} + 4CH_2 \rightarrow 3H_2S + 4H_2O + 4CO_2$ (2.3b)

Note that for the reduction by organic matter to occur, some H_2S is initially required as a catalyst. The H_2S produced is used for precipitation of PbS and ZnS. The kinetics of these

reactions pose no problem at temperatures exceeding 150 °C. The rate of sulphate reduction at temperatures below 150 °C is dependant on pH, fO_2, the activity of $(SO_4)^{2-}$ and the activity of the reducing agent (Ohmoto and Lasaga, 1982).

Destabilisation of organic complexes by reduced sulphur

Lead and zinc are transported in organic as well as chloride complexes together with reduced sulphur in one fluid. Reversible precipitation occurs as a result of destabilising these organic complexes by:
(1) oxidation (increase in fO_2);
(2) pH change;
(3) cooling; and
(4) dilution

All of these effects can, for example, be achieved by mixing with a colder, low-salinity meteoric aqueous solution. A problem with this model is that no proof has been found of any organic ligand that can significantly increase the solubility of lead and zinc (Sicree and Barnes, 1996).

POSSIBLE SOURCES OF MVT COMPONENTS

Brine source

Evaporation of seawater and/or halite dissolution may be possible mechanisms for the generation of basinal sedimentary brines. These two main mechanisms may not be mutually exclusive (Chi and Savard, 1997), and fluids produced by these processes may mix with one another as well as with meteoric water to explain variations in the geochemistry. Considering the long transport distances of up to several hundreds of kilometres (Cathles and Smith, 1983), it is also possible that brines are derived from orogenic belts, i.e., fluids attributed to magmatic or metamorphic processes (Duane and Saggerson, 1995).

Sulphur source

Organic material and/or sulphate minerals (both present at the site of mineralisation) may be possible sources of sulphur. Sulphur can, however, also be transported as reduced sulphur in a separate, non-metal-bearing fluid or as sulphate in a metal-bearing fluid to the site of ore deposition. Sources for reduced sulphur are indicated as crustal components from isotopic compositions (Leach and Sangster, 1993). Whatever the ultimate sulphur source may be, it can be many kilometres away from the site of mineralisation. In many cases, deposits may derive their sulphur from composite, and not single sources, even in multifaceted mixtures (Leach and Sangster, 1993).

Metal source

Basement rocks are considered to be the most likely source of lead and zinc, as indicated by Pb-isotope studies (Heyl et al., 1974). These metals may also be derived from the sedimentary basin or from leaching of metals from the aquifers through which the brines migrated (Leach and Sangster, 1993). During the course of fluid migration, lead may be leached from alkali feldspars, whereas clays, micas, pyroxenes, and amphiboles may release zinc, copper, and tin (Skinner, 1997). As discussed by Leach and Sangster (1993), Zn/Pb ratios may be related to

host rock lithologies: sandstone-hosted ore deposits are often lead rich, whereas carbonate-hosted MVT deposits are typically zinc rich. An exception is the southeast Missouri MVT district, where carbonate-hosted deposits yield more lead than zinc. This may be explained by the presence of the basal sandstone, which is believed to be an important aquifer (Leach and Sangster, 1993). Therefore, it is suggested that host rocks may also be the aquifers through which the fluids migrated. It is important to note that metals might also be derived from multiple sources.

PERING Pb-Zn DEPOSIT

Of various known carbonate-hosted lead-zinc occurrences in the Transvaal Supergroup of South Africa, the Pering deposit in the Northwest Province (Fig. 6) is by far the largest and the only one that is currently mined at 2.10 wt.% Zn and 0.55 wt.% Pb. The expected life of mine is until 2004. Together with some smaller Pb-Zn deposits, including Bushy Park (Griquatown) and the F-Pb-Zn deposits of the Zeerust district, Pering has been classified as a Mississippi Valley-type deposit based on the geological setting, mineralogy, mineral chemistry, and the presence of hydrocarbons (Beukes, 1986; Martini, 1986; Wheatley et al., 1986; Roberts, 1992; Turner, 1992; Roberts et al., 1993; Martini et al., 1995, Greyling, 2000).

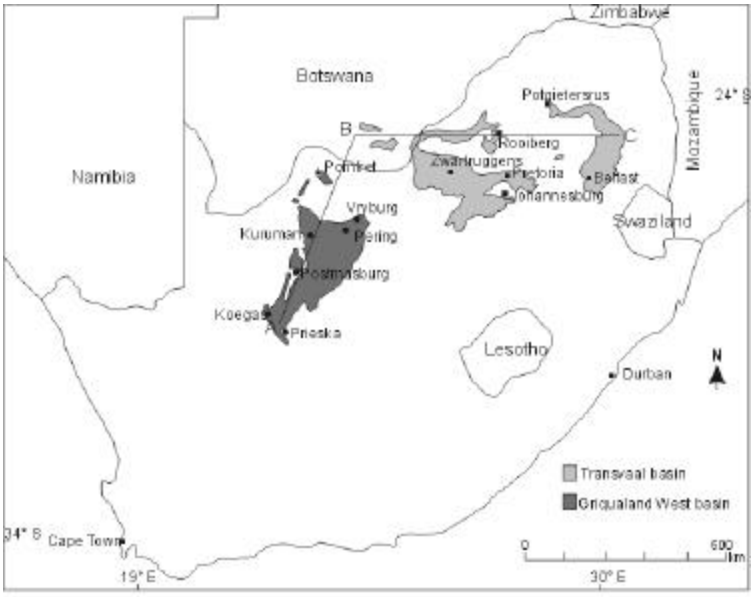

Figure 6 The Transvaal Supergroup preserved in the Griqualand West sub-basin and the Transvaal sub-basin, South Africa (after Beukes, 1978). The lines (A-B-C) are represented in figure 7 as a cross-section.

Pering and related deposits in the Chuniespoort-Ghaap dolomites are of specific importance as the oldest known MVT deposits, indeed as the only known deposits of Palaeoproterozoic age. The Late Archaean age for the stromatolitic dolomites of the Reivilo Formation was constrained by Barton et al. (1994), who determined an age of 2552 ± 11 Ma for dolomites stratigraphically below the Reivilo Formation in the Campbellrand Subgroup. Sumner and Bowring (1996) arrived at an age of 2521 ± 3 Ma for the Gamohaan Formation, which is at the immediate top of the Campbellrand Subgroup. This suggests a late Neoarchaean age for the deposition of the Campbellrand-Malmani carbonate platform (of the Ghaap/Chuniespoort Groups) which is, therefore, the oldest known extensively preserved carbonate platform in the world.

The precise age of mineralisation for the Pering deposit is not known, but Roberts et al. (1993) estimated the age of hydrocarbon migration and associated Pb-Zn mineralisation in the Ghaap/Chuniespoort Groups of the Transvaal Supergroup at between 2220 - 2060 Ma. Martini et al. (1995) suggested a similar age range (2350 - 2060 Ma) for the Zeerust F-Pb-Zn deposits based on stratigraphic arguments. An age of 2023 Ma for the Ghaap mineralisation was indicated by ore and gangue minerals by Kruger et al. (1999), where fluids were driven by the *c.* 2000 Ma Kheis fold and thrust belt on the western edge of the Kaapvaal Craton. Assuming that these estimates are correct, the deposits in the Transvaal Supergroup are the oldest known Mississippi Valley-type deposits worldwide. Attempts to directly date the hydrothermal mineralisation of the Pering deposit have remained unsuccessful (Rb-Sr dating of sphalerite; J. Kramers, pers. comm., 2000).

Regional geology

The Pering deposit occurs in the dolomites of the lower part (i.e., the Reivilo Formation of the Campbellrand Subgroup) of the Ghaap Group in the Transvaal Supergroup, which is preserved in the Griqualand West sub basin (Fig. 6).

The Transvaal Supergroup in South Africa is preserved in two structural basins, specifically the Transvaal basin and the Griqualand West basin (Fig. 6) (Altermann and Wotherspoon, 1995; Eriksson et al., 1995). This sedimentary assemblage is stratigraphically correlated in the Griqualand West and Transvaal basins (Fig. 7) (Beukes, 1986). Varying interpretations of this correlation by Beukes (1980, 1986, 1987) and SACS (1980) are discussed in detail in the publications of Altermann and Wotherspoon (1995) and Sumner and Bowring (1996). The Transvaal Supergroup consists of 2700-2200 Ma old sedimentary and volcanic rocks that unconformably overlie the Ventersdorp Supergroup (Beukes, 1978; Trendall, 1990; Barton et al., 1994). Deposition of the Transvaal Supergroup extended over an area of 500 000 - 600 000 km^2 (Tankard et al., 1982; Beukes, 1987; Altermann and Wotherspoon, 1995). The Transvaal Supergroup in Griqualand West (Fig. 8) is represented by the chemical sedimentary Ghaap Group, which is unconformably overlain by the volcano-sedimentary Postmasburg Group (Fig. 9) (Beukes, 1978, 1983, 1986). The red beds of the Olifantshoek Supergroup unconformably overlie the Transvaal Supergroup in the Griqualand West area.

The Ghaap Group in the Griqualand West basin correlates with the Chuniespoort Group in the Transvaal basin and consists predominantly of limestone, dolomite, chert, and iron-formation (Button, 1973; Eriksson and Truswell, 1974; Beukes, 1986; Martini et al., 1995; Sumner and Bowring, 1996). The Ghaap Group is subdivided into the Schmidtsdrift Subgroup (interbedded siliciclastics and carbonate rocks), the Campbellrand Subgroup (limestones and dolomites), the Asbesheuwels Subgroup (iron formation) and the Koegas Subgroup (interbedded siliciclastics and iron formation) (e.g., Beukes, 1978, 1986). Figure 9 shows a detailed stratigraphic section and correlation of the Transvaal Supergroup preserved in the Griqualand West and Transvaal basins. Deposition of the Ghaap Group in Griqualand West occurred under conditions pertaining to a shallow-water platform on the Kaapvaal Craton and a deeper water basin on the southwestern and western edge of the platform (see Fig. 7) (Beukes, 1978; Tankard et al., 1982).

The deposition of the Campbellrand Subgroup occurred on a shallow marine platform and is bounded by the argillitic Lokammona Formation of the Schmidtsdrift Subgroup at the base and the Kuruman Iron Formation of the Asbesheuwels Subgroup at the top (Figs. 7 and 8) (Beukes, 1980, 1986). The chemical-sedimentary Campbellrand Subgroup (in the Griqualand West basin) is correlated with the Malmani Subgroup (in the Transvaal basin) and represents a carbonate build-up from 2552 ± 11 Ma (Barton et al., 1994) to 2521 ± 3 Ma (U-Pb age -

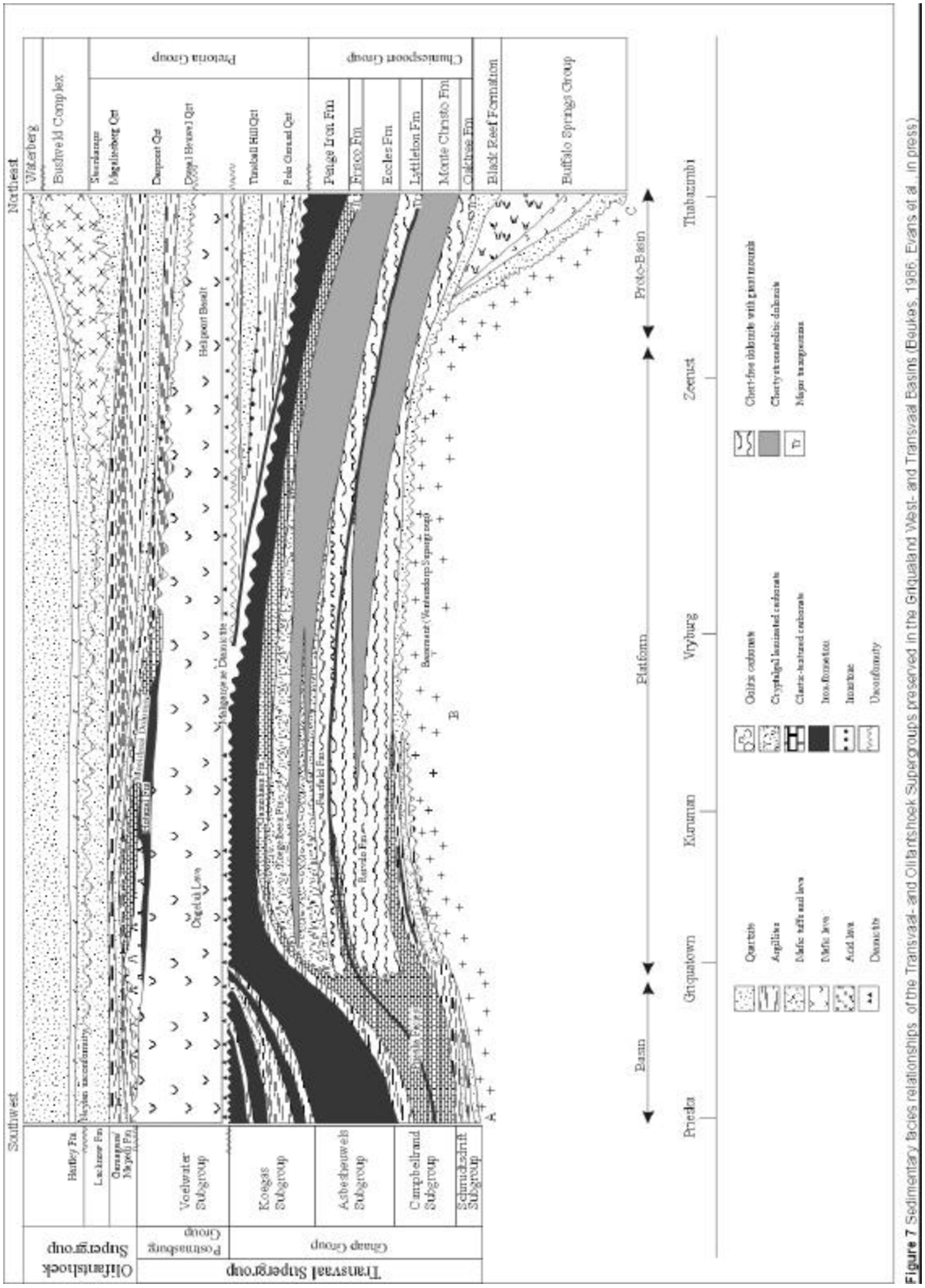

Figure 7 Sedimentary facies relationships of the Transvaal- and Olifantshoek Supergroups preserved in the Griqualand West- and Transvaal Basins (Beukes, 1986; Evans et al., in press)

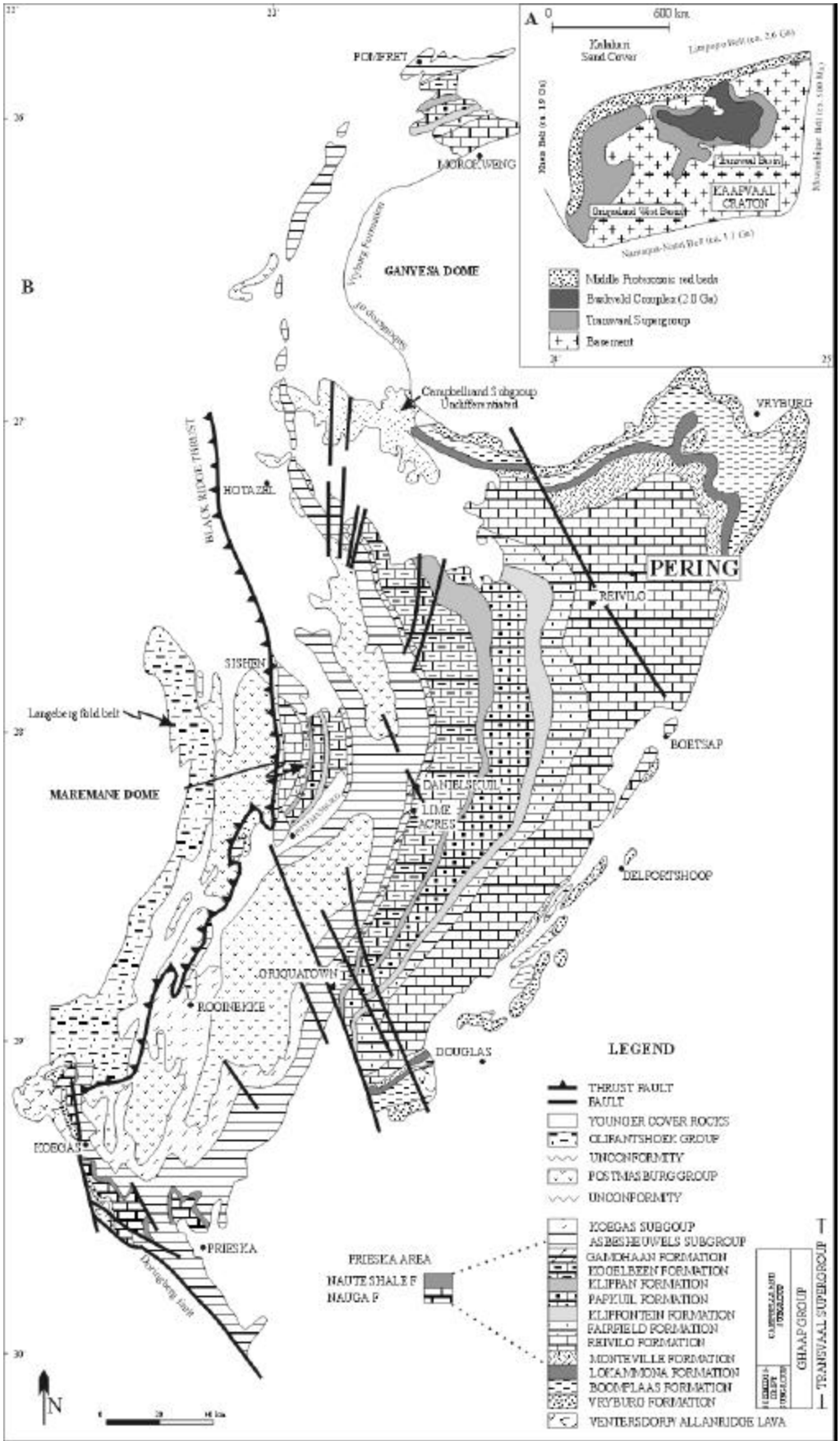

Figure 8 The locality and general geology of Griqualand West (after Beukes, 1983).

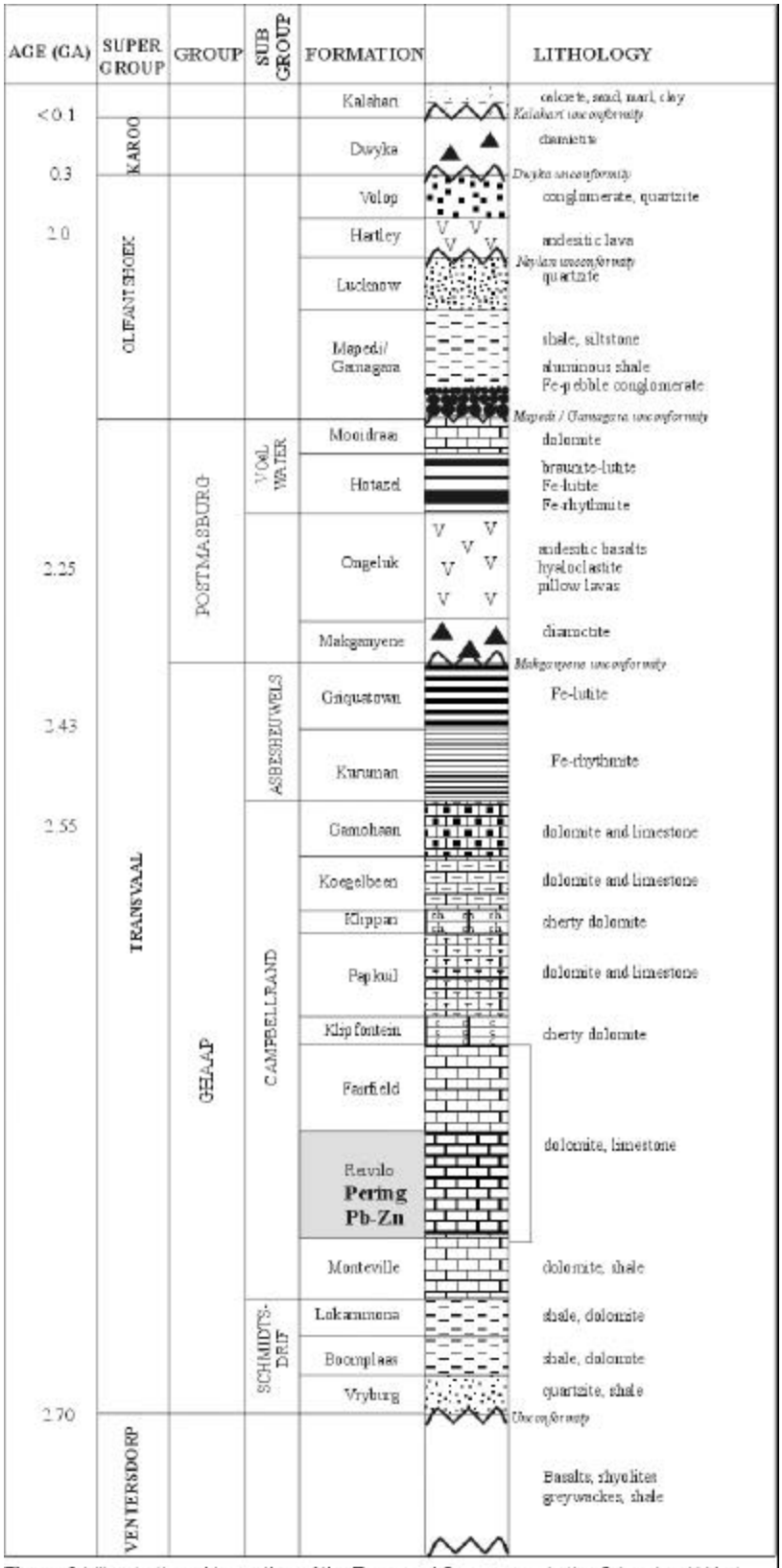

Figure 9 Lithostratigraphic section of the Transvaal Supergroup in the Griqualand West area representing the platform lithofacies (Gutzmer, 1996 and references therein; Dorland pers. comm., 2000)

Sumner and Bowring, 1996). Two major lithofacies assemblages are recognised in this succession, namely a basinal carbonate-shale sequence off the craton to the south, in the Prieska area (Fig. 8), and a shallow-water carbonate platform sequence on the craton proper (Beukes, 1986, 1987).

The Campbellrand Subgroup is divided into the Monteville, Reivilo, Fairfield, Klipfontein, Papkuil, Klippan, Koegelbeen and the Gamohaan Formations (SACS, 1980). The basinal sequence consists of non-stromatolitic, laminated carbonate and shale with minor chert, iron-formation and mafic tuff beds, while the sequence on the craton proper comprises shallow water stromatolitic carbonates of a limestone platform facies (Beukes, 1980, 1987). The Campbellrand Subgroup has been completely dolomitised in the lagoonal, intertidal, and supratidal environments on the platform interior (Beukes, 1986). The platform margin was maintained by growth faults along the edge of the craton. This marginal facies is defined by columnar stromatolites, oolites, carbonate arenite shoal deposits (Beukes, 1987) and limestone-rich zones (Beukes, 1978).

The basal and top sections of the Campbellrand Subgroup are characterised by thin intercalations of black shale, while light-coloured, cherty dolomite predominates in the central section of the Subgroup. The distal facies of the carbonate turbidites has been ankeritised and partly replaced by silica, producing banded ferruginous cherts. These interfinger with carbonaceous shale deposited in an euxinic environment. Carbonate deposition on the Kaapvaal Craton ceased due to a transgression after which the Kuruman iron-formation (consisting of deeper water, micro- banded ferhythmites) was deposited.

Reivilo Formation

The Reivilo Formation is subdivided, according to Beukes (1978), into six zones that are classified on the base of facies-changes. These zones are the giant domal stromatolitic Ulco Member (Zone 1), followed by the giant domal- and columnar-stromatolitic dolomites of the Steekdorings Member (Zone 2) (Fig. 10). The columnar stromatolites may interfinger with the giant domal stromatolites or may be separated by thin crossbeds of ripple-marked dolomite and interbedded carbonaceous shales. The Steekdorings Member is overlain by giant domal stromatolites of Zone 3, followed by the light-coloured, coarse-crystalline, wave-laminated dolomite, oolitic dolomite and dolarenite of Zone 4. Zone 5 is mostly constructed of giant domal stromatolitic dolomite with intercalated ripple-cross-bedded dolarenite. Zone 6 is the Kamden Member and is essentially laminated iron-rich dolomite. The Reivilo Formation conformably overlies the quartz-arenitic Motiton Member of the Monteville Formation, while the top of the Reivilo Formation consists of a cherty ferruginous dolomite unit (Fig. 9) (Beukes, 1978).

The sedimentary environment for the deposition of the dolomites of the Pering Pb-Zn deposit was a low-energy, subtidal-intertidal, shallow-water environment of the Steekdorings Member of the Reivilo Formation. This environment was stable with extensive lagoonal mud flats interfingering with coastal sabkhas, with the open sea to the southwest. A cyclic pattern is present in the form of several periodic transgressions (e.g., Klein and Beukes, 1989).

Figure 10a Domal stromatolites of Stromatolite zone 1, of the Steekdorings Member of the Reivilo Formation exposed in the Pering open pit.

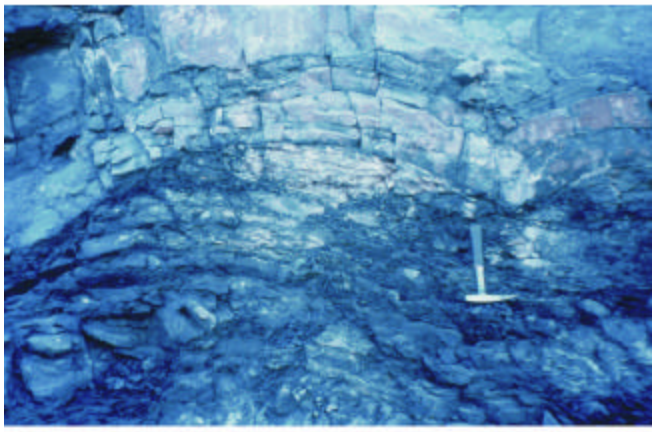

Figure 10b Giant domal stromatolites of Stromatolite zone 2, of the Steekdorings Member.

Pering Sequence in the Steekdorings Member

Epigenetic, disseminated, stratabound Pb-Zn mineralisation is hosted by several texturally distinct units of the Steekdorings Member of the Reivilo Formation. Late-stage brecciation of the dolomite host rock, and the associated ore mineralisation are preserved as crosscutting breccia bodies (Fig. 11). The structural geology around the unmetamorphosed Pering deposit is simple. The regional dips of the dolomite host rocks are subhorizontal (Wheatley et al., 1986). A circular basin-like structure (~2 km in diameter), with dips of ~10° to 20° towards its centre, defines the position of the ore body (Wheatley et al., 1986). North-south trending faults and/or fractures occur in the vicinity of the deposit (Fig. 12). The ore body (in the centre of the basin-like structure) is centred around two roughly oval-shaped hydrothermal breccia bodies (the Central- and Southern Breccia bodies) of 200-300 m in diameter (SSAM, 1988). Three breccia bodies (the Southern, Central and subordinate Northern Breccia bodies) crosscut the stratigraphy both vertically and laterally.

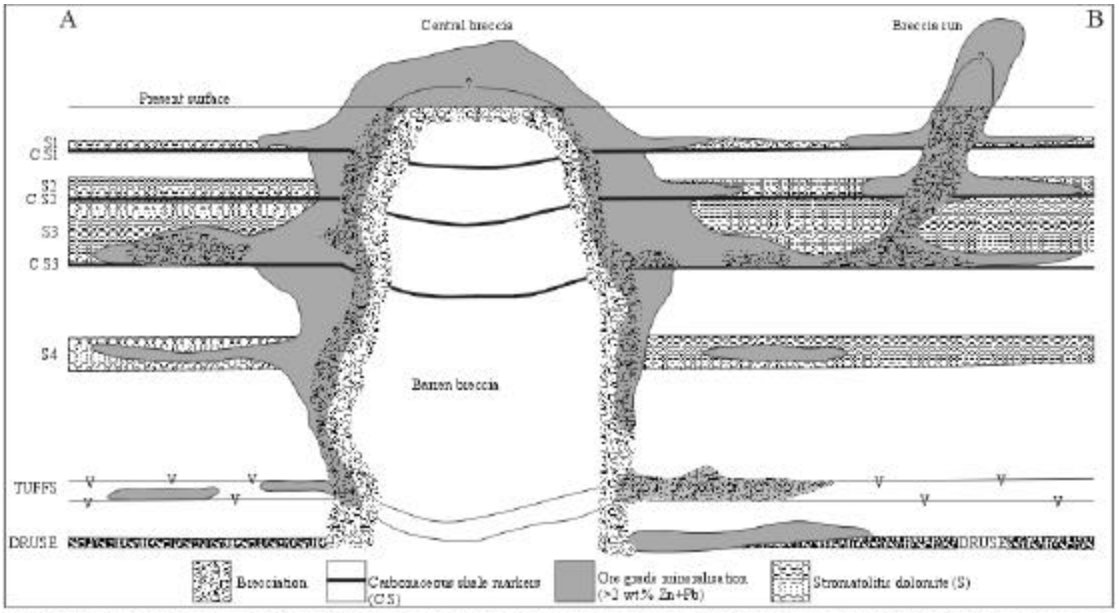

Figure 11 Schematic cross-section of the Pering orebody by Wheatley et al. (1986) indicating the ore mineralisation presented with the stromatolitic units, carbonaceous shale marker horizons, tuffs and druse with associated intermittent dolomite units (unshaded). See figure 13 for stratigraphic section and text for description of related stratigraphic sequence. Figure 12 illustrates the plan-view of the cross-section.

The mineralised part of the Steekdorings Member is locally known as the Pering Sequence (Wheatley et al., 1986) (Fig. 13), preserved in several dolomite units or zones. These include:

Druse

The druse zones are subdivided into upper (U.Druse), middle (M.Druse) and lower (L.Druse) zones according to their stratigraphic position. Post-depositional dissolution (possibly of stromatolitic units) has generated large volumes of porosity, partly filled by coarse-crystalline quartz, sparry dolomite, and late sphalerite (Sp-III[4]) and galena (Gn-II) mineralisation. Some occurrences of disseminated sphalerite (Sp-I) were also noted in the drusy dolomite;

Lower massive dolomite (LMD)

The massive dolomite zones are subdivided according to their stratigraphic position, e.g., upper massive (UMD), massive (MD), and lower massive (LMD). These zones are fine-grained medium- to light-grey coloured, massively textured dolomites, with some dissolution and replacement of fine-grained sparry dolomite and calcite. Concretionary diagenetic pyrite nodules (ranging in size from 5-20 mm) are present throughout this zone;

Tuff

Layers of mafic tuff are intercalated with massive- and laminated-algal dolomite. These tuff layers vary from ~2 cm to ~10 cm in thickness and have a distinct greenish-grey colour and a fine-grained massively textured appearance;

Stromatolite zone 5 (S5)

This zone consists of medium-grey massive dolomite, with occasional columnar stromatolites. The stromatolitic layers are accentuated by sparry dolomite infills. First-generation disseminated sphalerite (Sp-I) mineralisation is mostly restricted to these stromatolitic layers. The last sphalerite (Sp-III) and galena generations (Gn-II) are present as euhedral crystals in vugs together with saddle-shaped hydrothermal dolomite crystals.

[4] See Mineralogy section.

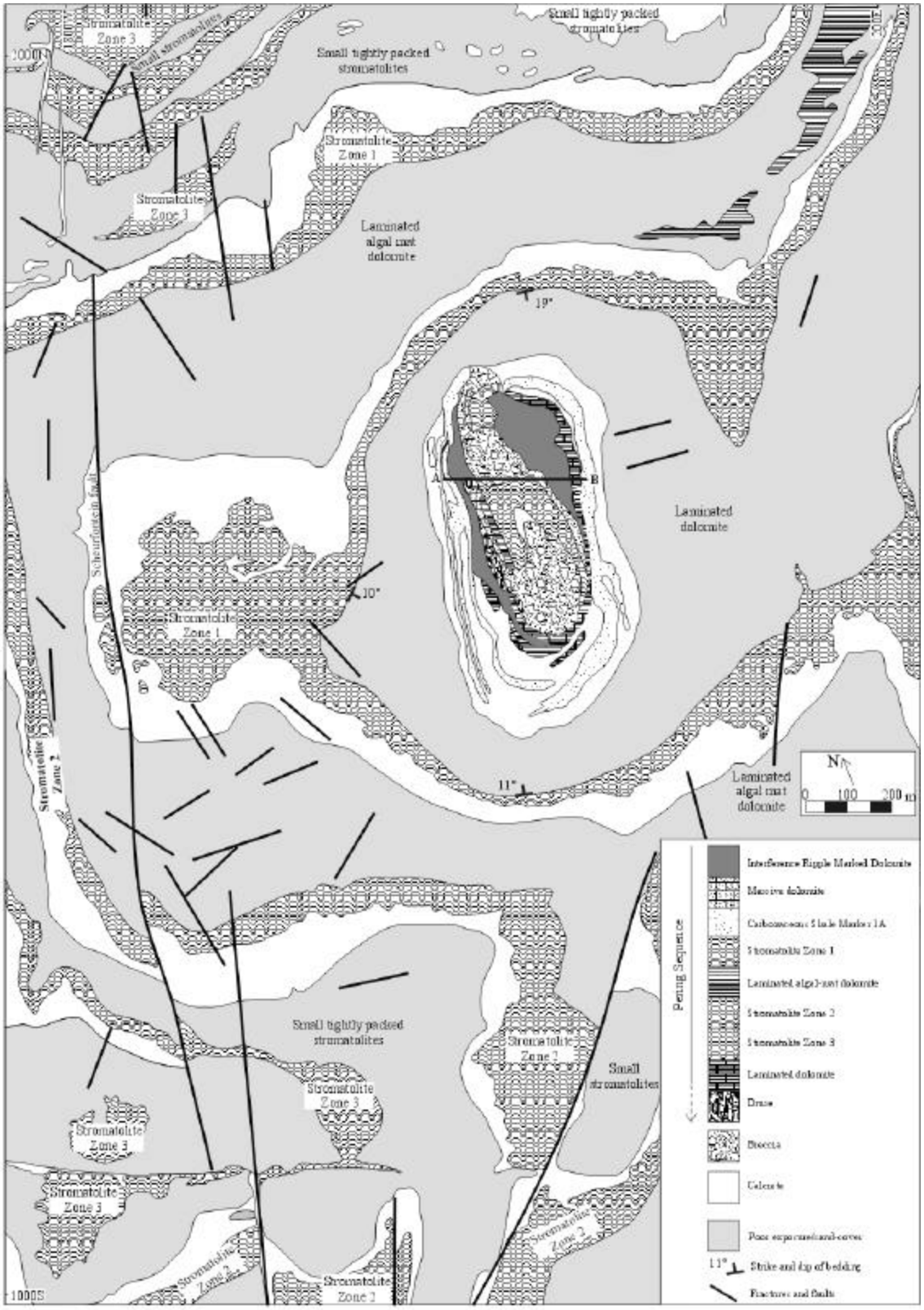

Figure 12 Geological map of the Pering orebody and surrounding area (27° 31'S, 24° 13'E) with the local mine grid presented on the figure (modified after SSAM, 1986). See figure 13 for the stratigraphic profile, and text for a generalised description of individual zones. Line A-B is the position of the cross section of the orebody (after Wheatley et al., 1986) illustrated in figure 11.

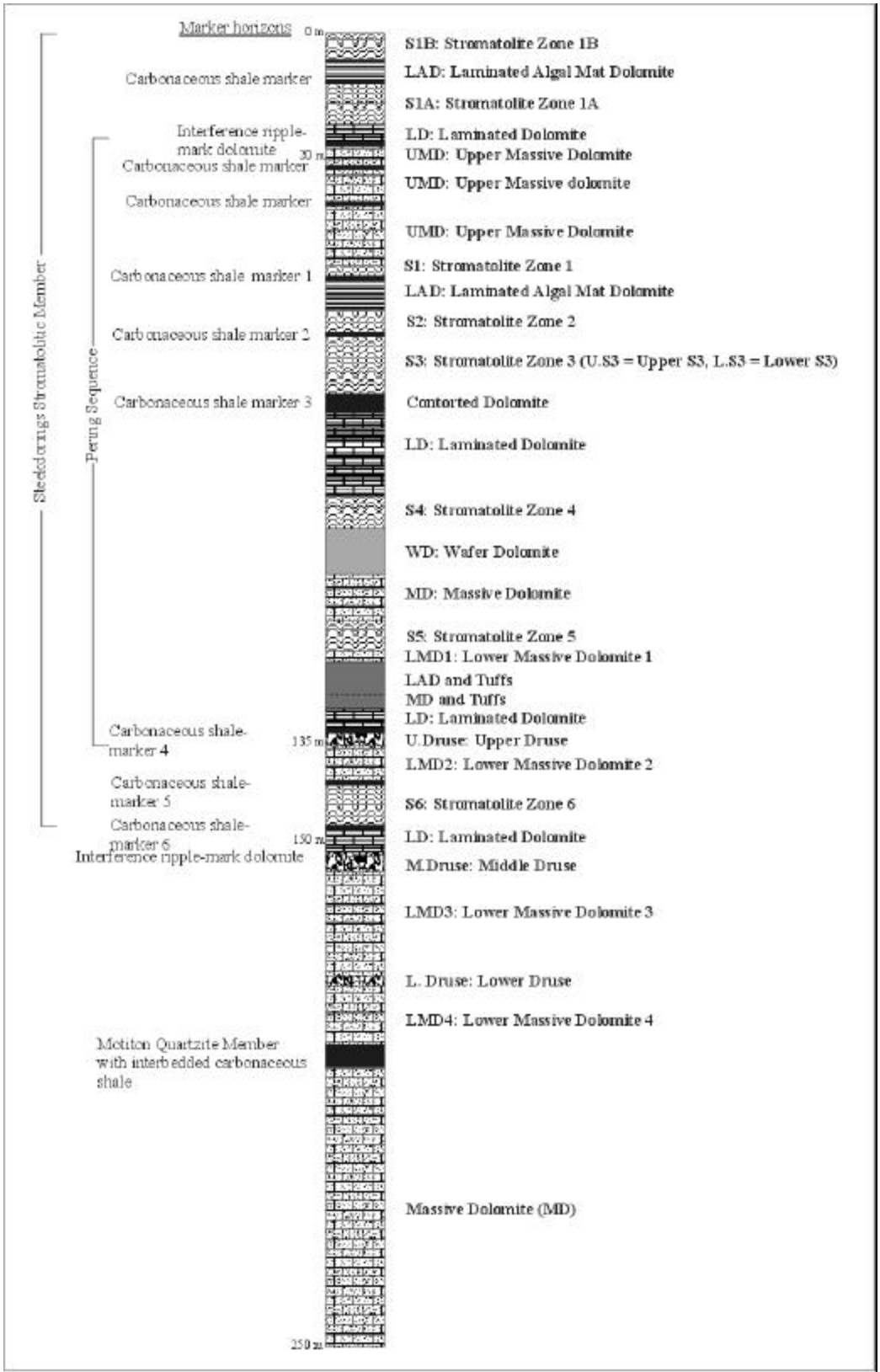

Figure 13 Generalised stratigraphic section of the Pering Sequence as described by Wheatley et al. (1986). Marker horizons are indicated in solid black. A generalised description of each zone is given in the text.

Wafer dolomite (WD)

Dolomite in this zone has a medium-grey colour, with a massive texture, and was dissolved and fractured during the first brecciation event (B-1[5]). These breccia fragments are cemented by sparry dolomite. Calcite is present as open-space infill, with occasional associated organic material. Late-stage mineralisation of sphalerite and galena (Sp-III and Gn-II) mostly occurs as open-space infill, together with calcite- and saddle-shaped hydrothermal dolomite crystals in vugs related to late brecciation (B-3);

Stromatolite zone 4 (S4)

Small-scale brecciation (B-1) of the dolomite host rock is characteristic of this zone. Dolomite host rock fragments are cemented by sparry dolomite, together with some calcite veins that randomly crosscut the unit. Disseminated sparry dolomite and fine-grained sphalerite (Sp-I) are mostly restricted to stromatolite layers. This unit is marked by an abundance of columnar stromatolites. Small diagenetic pyrite nodules are common. Vugs in the dolomite host are filled or partly filled with quartz and calcite;

Stromatolite zone 3 (U.S3 and L.S3)

Zone 3 is divided into an upper stromatolite zone 3 (U.S3), and a lower stromatolite zone 3 (L.S3). Both these zones are composed of medium-grey coloured dolomite displaying columnar stromatolitic textures. Sparitic dolomite and finely disseminated early mineralisation of sphalerite (Sp-I) and galena (Gn-I) persist along these stromatolitic layers. Secondary vugs in the dolomite host rock are filled or partly filled by saddle-shaped crystals of sparitic dolomite and occasionally late-stage galena (Gn-II) and calcite;

Stromatolite zone 2 (S2)

This dolomite unit is medium grey in colour. Disseminated, first-generation sphalerite (Sp-I) occurs, followed by vein infills of second generation sphalerite (Sp-II), that are found as rims around Sp-I mineralised breccia fragments. Sparitic dolomite replaces columnar- and domal-stromatolitic textures (Fig. 10b), and small-scale brecciation is locally present. Galena (Gn-II) is concentrated in veins of sparry dolomite;

Stromatolite zone 1 (S1)

A medium- to light-grey-coloured zone of micritic dolomite, occasionally with some domal stromatolites present, is shown in Figure 10a. This zone generally hosts no ore mineralisation. The dolomite host is partly replaced by sparry dolomite, and secondary vugs are lined by saddle- dolomite crystals. Sparry dolomite occurs disseminated along stromatolite horizons and is concentrated in large, irregular-shaped pods. Thin shale horizons (~20 mm thick) and abundant diagenetic pyrite nodules are present;

Massive dolomite (MD)

This zone is composed of massive, fine-grained, medium- to light-grey-coloured dolomite, with some open-space infill of sparry dolomite and calcite. Thin intercalations of shale (5-10 mm thick) are present throughout the zone, with diagenetic pyrite nodules locally scattered throughout this zone. Although the zone is generally devoid of Pb-Zn mineralisation, veins of sparry calcite with late-stage galena (Gn-II) have been found;

Laminated dolomite (LD)

Medium- to light-grey-coloured, micritic dolomite is characteristic of this zone, with laminations of more massive-textured dolomite increasing toward the lower section of this zone. Thin laminations rich in organic material are present, together with concretionary diagenetic pyrite nodules;

[5] See Mineral paragenesis section.

Laminated algal dolomite (LAD)

This zone comprises light- to medium-grey-coloured, micritic dolomite, with occasional sparry dolomite veins running bedding-parallel, as well as crosscutting the bedding planes. Nodules of bitumen are present in late sparitic calcite vug-infills. Calcite veins appear to be spatially associated with diagenetic pyrite nodules ranging in size from 2-3 cm in diameter;

Upper massive dolomite

This zone consists of micritic dolomite, with intercalated shale horizons. It is usually not well mineralised with sphalerite and galena. However, some areas of finely disseminated sphalerite (Sp-I) mineralisation have been identified and are associated with epigenetic dissolution of the dolomite host rock.

Mineralogy and petrography

Lead and zinc mineralisation commonly occurs as finely crustiform-colloform-textured material in stromatolitic horizons, with minor late mineralisation present as coarse-crystalline, open-space infill in several distinct hydrothermal breccia bodies that crosscut the stratigraphy. The most abundant ore minerals in both types of mineralisation are low-Fe sphalerite and low-Ag galena. Sphalerite clearly predominates over galena in abundance (Fig. 1c). Trace amounts of chalcopyrite are associated with the Pb-Zn mineralisation. The gangue minerals are quartz, calcite, and dolomite, with diagenetic pyrite concretions abounding in the dolomites of the Campbellrand Subgroup. Weathering of the upper part of the ore body resulted in the formation of supergene minerals, e.g., smithsonite, hydrozincite, cerussite, anglesite, secondary galena, descloizite and calcite (Southwood, 1986). The formation of these minerals coincided with sulphide dissolution and dedolomitisation of the host rock.

Mineral paragenesis

Ore minerals identified in the Pering deposit include sphalerite, galena and chalcopyrite. Pyrite occurs as diagenetic concretionary nodules (Beukes et al., 1990), and is therefore not part of the hydrothermal mineral assemblage. Gangue minerals include pyrite, secondary sparry dolomite, quartz, and calcite. Oil residues were found in doubly polished quartz sections, and bitumen is abundantly present either as small nodules, or as coatings on the dolomite host rock. The relative chronology of ore and gangue mineral formation is presented in Table 2.

The dolomite host rock is affected by three hydrothermal events of dissolution and brecciation. These three brecciation events are manifested by three texturally distinct sphalerite generations clearly observed in hand-specimen and field exposures. The first generation of sphalerite (Sp-1) occurs as disseminated crustiform-colloform-textured mineralization dark-brown in colour. The second sphalerite generation (Sp-II) is present as rims around brecciated fragments, with the third generation (Sp-III) appearing as coarse, open-space infills in vugs. These brecciation events are further characterised by fragments of dolomite host rock and hydrothermal mineralisation cemented by successive generations of hydrothermal sulphides, carbonates, and quartz:

(B-1) Brecciation of the dolomite host rock, and first introduction of hydrothermal sparry dolomite. This event occurs prior to, or during, disseminated Sp-I and Gn-I mineralisation.

(B-2) Brecciation of the dolomite host rock, hydrothermal dolomite, Sp-I, and Gn-I, and further introduction of hydrothermal sparry dolomite. This event occurs prior to, or during, Sp-II precipitation.

(B-3) Brecciation of the dolomite host rock, hydrothermal dolomite, Sp-I, Gn-I, and Sp-II. This event predates Sp-III, Gn-II, quartz, and calcite precipitation.

Table 2: Mineral paragenesis chart

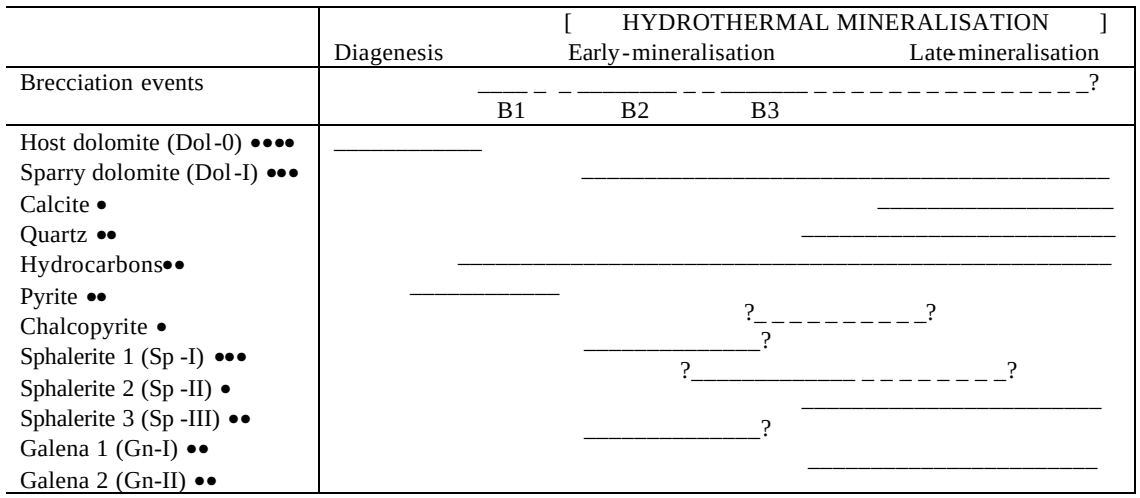

Abundance: • rare, •• fairly abundant, ••• medium abundance, •••• most prevalent

Early mineralisation (postdating the first brecciation event B-1 and introduction of sparry dolomite, which cements fragments of dolomite host rock) occurs as crustiform-colloform textured, finely disseminated sphalerite (Sp-I) and galena (Gn-I), hosted mostly by stratabound ore bodies along stomatolitic units of the dolomite host rock. These stratabound ore bodies are essentially subhorizontal breccia bodies, with minor brecciation. This early mineralisation episode in the stratabound ore bodies is associated with the first brecciation event (B-1), and ceased prior to the second introduction of sparry dolomite. After this initial episode, a second, minor brecciating event (B-2) followed, with rims of a second generation of sphalerite (Sp-II) formed on the dolomite host rock and on Sp-I. Formation of Sp-II was followed by brecciation event B-3. B-3 signals late stage mineralisation characterised by coarse-crystalline, open-space fills of sphalerite (Sp-III) and galena (Gn-II), and contemporaneous crystallisation of sparry

dolomite and quartz. This is mostly restricted to crosscutting breccia pipes/bodies. Calcite precipitation occurs last as open-space infill in hand specimen, and as veins crosscutting the sparry dolomite on a microscopic scale.

Gangue minerals

Dolomite host rock (Dol-0)

The host rock varies from dark- to light-blue-grey colour in hand specimen, with a fine- to very fine-grained, uniform texture (Leighton and Pendexter, 1962). The host is composed of more than 90% dolomite (showing no presence of allochems, with less than 10% calcareous textures) (Leighton and Pendexter, 1962), with layers of dolomitized domal (Fig. 10) and columnar stromatolites. Stylolites, with typical saw-teeth shapes, are present within the dolomite. The varying colour of the host is due to differing amounts of poorly crystalline graphite present in the dolomite as indicated by Raman microspectrometry (Pasteris and

Wopenka, 1991). The dolomite host contains traces of SiO_2 (<1 wt.%), FeO (<2 wt.%) and MnO (<3 wt.%).

A dull red luminescence colour is apparent (Fig. 14a). Disseminated Sp-I and Gn-I pervade the host rock along stromatolitic units. Dissolution along stromatolitic layers resulted in the replacement of the dolomite host rock by secondary sparry dolomite. Fractures and veins of sparry dolomite crosscut massively textured dolomite host rock. The dolomite host, as well as the early mineralisation (Sp-I, Sp-II and Gn-I), was affected by the subsequent B-2 brecciation event. Angular dolomite host fragments - as well as partly dissolved dolomite host fragments and Sp-I, Sp-II and Gn-I - "float" in a matrix of sparry hydrothermal dolomite, which postdates the last brecciation event (B-3).

Hydrocarbons

Hydrocarbons are widespread, minor constituents, occurring as scattered opaque fragments in thin section (generally averaging ~20 µm in size) and hand specimen within the dolomite host rock and sphalerite (Sp-I). Raman microspectrometry identified these fragments in the dolomite host rock as poorly crystalline graphite (Pasteris and Wopenka, 1991). Some opaque material
was also Raman inactive, and is therefore probably bitumen. Late-stage hydrocarbons (also poorly-crystalline graphite) are associated with quartz, sphalerite (Sp-III), and hydrothermal sparry dolomite (Fig. 14b). The core of the hydrocarbon nodule shown in Figure 14b is oil, while the outer rim of the nodule is bitumen and/or poorly crystalline graphite as determined by ultraviolet microscopy and Raman microprobe (Pasteris and Wopenka, 1991).

Hydrothermal dolomite (Dol-I)

Hydrothermal dolomite abounds throughout the Pering ore body. It occurs as: (1) disseminated sparry[6] dolomite, which replaces dolomite host rock (Dol-0); (2) sparry dolomite cement (related to B-1 and B-3) amid fragments of dolomite host rock and earlier hydrothermal mineralisation; (3) veins of sparry dolomite, crosscutting the host rock, Sp-I, Gn-I, and Sp-II; (4) open-space infill (partly or complete) of euhedral saddle-shaped crystals of sparry dolomite together with Sp-III and/or Gn-II; and (5) dolomite inclusion trails (individual inclusions ranging in size from 10 - 50 µm) in quartz (Fig. 14c).

These inclusions were identified as dolomite with cathodoluminescence microscopy. The different occurrences of sparry dolomite indicate that secondary hydrothermal dolomite was formed continuously from the first brecciation event (B1) up until late mineralisation, marked by the formation of Sp-III and Gn-II.

Two texturally different hydrothermal sparry dolomite types are discernible by cathodoluminscence microscopy and Alizarin Red-S–PF staining. Distinction between the two sparry dolomite types is based on the observation that one exhibits a homogeneous luminescence colour, whereas the other shows distinct oscillatory growth zoning that is probably due to variations in iron and/or manganese content (Fig. 14d) (Machel and Burton, 1991). Macroscopic distinction between the two generations is arduous without the aid of cathodoluminescence microscopy and/or Alizarin Red-S–PF staining. Sparry dolomite contains traces of SiO_2 (<1 wt.%), FeO (<3wt.%) and MnO (<3 wt.%), which is similar to the mineral chemistry of dolomite in the host rock.

[6] Refers to clear, transparent or translucent, readily cleavable, crystalline particles generally having an interlocking mosaic texture (Leighton and Pendexter, 1962), with grain size generally >4 µm (Folk, 1959). 'Spar' refers to crystal sizes including microspar (4-50 µm) and pseudospar (>50 µm) (Bathurst, 1975).

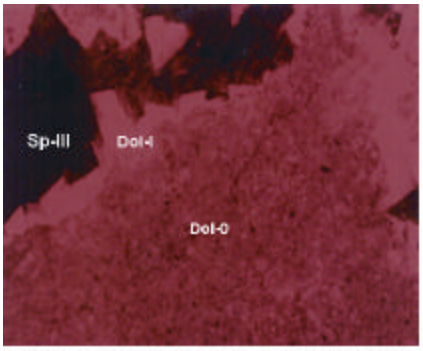

Figure 14a Cathodoluminescence image of dolomite host rock (Dol-0), showing dull red luminescence, rimmed by hydrothermal dolomite (Dol-I) in thin section taken from diamond drill core P1, at 107.4 m depth. The base of the image corresponds to 0.8 mm.

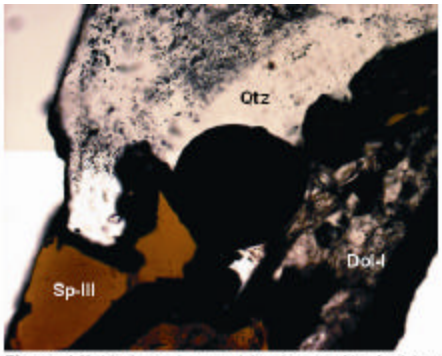

Figure 14b Hydrocarbon nodule observed in doubly polished section in transmitted light (sample P2-3(2), 200 mm thick). When studied in ultraviolet light, the core of the nodule luminesces yellow, indicating the presence of oil, whereas the outer rim shows no luminescence, indicative of graphite or bitumen. Base of the image corresponds to 2.6 mm.

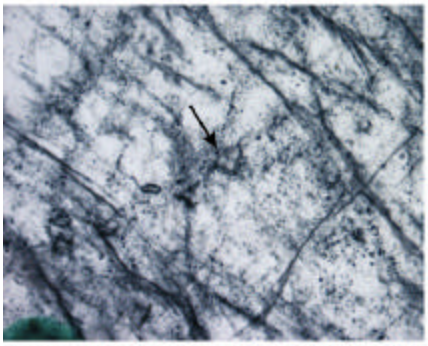

Figure 14c A trail of euhedral dolomite inclusions (arrow) (parallel to the growth zone) hosted in quartz as seen in a doubly polished thin section (200 mm thick), sample P2-3(2), suggesting that dolomite precipitation occurred contemporaneously with quartz precipitation from the hydrothermal fluid. Base of image corresponds to 2.6 mm.

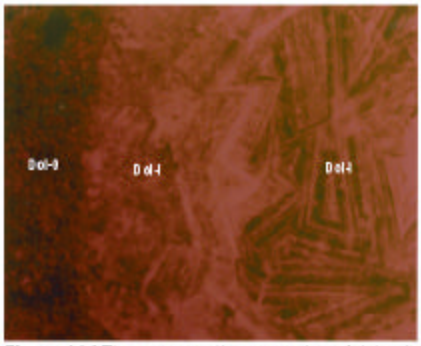

Figure 14d The paragenetic succession of dolomite host rock (Dol-0), and hydrothermal dolomite (Dol-I) viewed with cathodoluminescence, sampled from diamond drill core P1,at 37 m depth. Note the oscillatory vs. non-oscillatory nature of the hydrothermal dolomite. Base of the image equals 0.8 mm.

Figure 14e Euhedral crystals of quartz as open-space infill together with saddle-shaped hydrothermal dolomite crystals. The prominent quartz crystal in the foreground equals 4 cm in the vertical dimension. Hand sample P2-6.

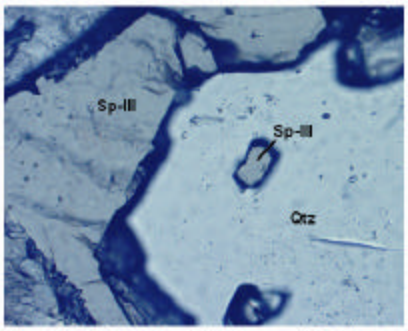

Figure 14f Transmitted-light image of Sp-III enclosed in quartz suggesting the co-precipitation of Sp-III and quartz. Viewed in double polished thin section P899-9B. Base of image corresponds to 1.3 mm.

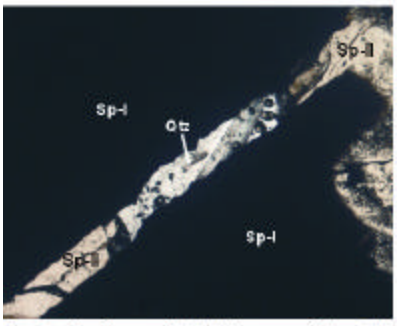

Figure 14g Transmitted-light image of a typical segmented vein of quartz and Sp-II crosscutting Sp-I. Quartz and Sp-II fill the vein simultaneously. Sample P899-9B. The base of the image corresponds to 2.6 mm.

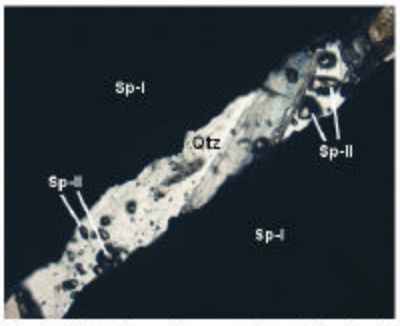

Figure 14h Enlarged image of figure 14g, showing quartz and Sp-II as a segmented vein in Sp-I. The base of the image corresponds to 1.3 mm.

Quartz

Transparent, euhedral quartz crystals, ranging in size from ~5 mm – ~10 cm (Fig. 14e) are encountered as a common constituent together with Dol-I, Sp-III, Gn-II and/or calcite as open space infill in the hydrothermal breccia bodies. Quartz is far less prevalent than hydrothermal dolomite in the Pering ore body. Figure 14 (c, f, g and h) illustrate the chronology between quartz, Sp-II, Sp-III, and Dol-I: quartz forms contemporaneously with Sp-II, Dol-I, and Sp-III.

Calcite

Two types of calcite were identified based on hand specimen examination. The first type (Cal-I) shows a typical milky appearance, with perfect rhombohedral cleavage, and is by far more abundant than the second calcite type (Cal-II), which is transparent. When stained with combined Alizarin Red S and potassium ferricyanide, both types show a pink- to red-brown colour, indicating a non-ferroan composition (Adams et al., 1984). Both calcite types show a bright orange luminescence.

Both types occur as infill and lining of vugs, distinctly younger than sparry dolomite, quartz, and Sp-III. Sp-III also occurs as inclusions (<1 mm diameter) in Cal-II. Calcite also infiltrates the sparry dolomite in vein-like fashion. There is no apparent consistent chronological relationship between the two calcite types.

Pyrite

Pyrite abounds as small concretionary nodules (ranging in size from a few mm's to ~3 cm) in the dolomite host rock, and also in intercalated shale units. Its characteristics are very similar to diagenetic pyrite nodules at other stratigraphical levels in the Campbellrand Subgroup (Klein and Beukes, 1989; Beukes et al., 1990). Figure 15a illustrates the porous appearance of such a concretionary pyrite nodule.

Ore minerals

Chalcopyrite

Chalcopyrite is a rare constituent that occurs closely associated with Sp-III and Gn-II as coarse- crystalline, open-space infill restricted to breccia bodies. Euhedral crystals up to 5 mm in size were recognised.

Sphalerite I (Sp-I)

Sp-I is the governing ore mineral present at the Pering ore body. Sp-I occurs macroscopically as dark-brown, fine-grained, crustiform-textured, colloform-banded to massive-granular aggregates, coating and replacing the host rock dolomite (Fig. 15b,c) after the first brecciation event (B-1). Sp-I often replaces sparry dolomite (Fig. 15d). Minute euhedral grains (< 50 μm) of galena are often found to dress certain growth bands of the colloform Sp-I. Colloform Sp-I is generally rimmed by Sp-II (after B-2) (Fig. 15e,f). Aggregates of Sp-I, Sp-II and Gn-I and host rock dolomite were subsequently brecciated by B-3 and cemented by late sparry dolomite. The distinct colloform texture of Sp-I may suggest precipitation of tiny, fibrous crystals from a supersaturated hydrothermal fluid.

Each colloform band reflects a distinct episode of crystal growth, separated by episodes of non-deposition, or a change of fluid chemistry. The bands are thought to have originated as radiating masses of minute crystals growing from many adjacent sites, for example along a vein wall or the surface of a wall rock fragment (as described in detail by Craig and Vaughan, 1994). This growth mechanism is illustrated in Figures 15 (g, h) and 16 (a-c). Sp-I contains less than 1 wt.% Fe (Fig. 17). The dark colour of Sp-I is attributed to the presence of amorphous graphite (and possibly hydrocarbon fragments) observed microscopically, and

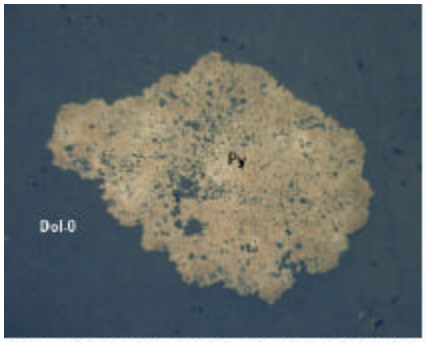

Figure 15a Reflected light micrograph, illustrating a nodular, spongy pyrite (Py) in the dolomite host rock (Dol-0). Sampled from core P9, at 103 m depth. Base of image corresponds to 1.3 mm.

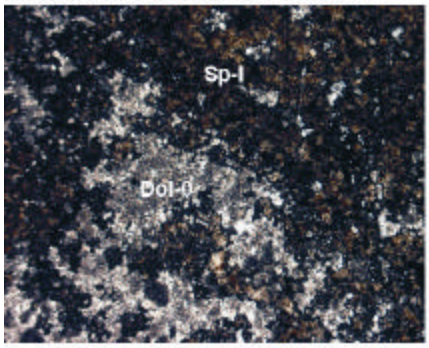

Figure 15c Disseminated Sp-I in the dolomite host rock (Dol-0) as observed in transmitted light (thin section sample P4-24). The base of the image corresponds to 2.6 mm.

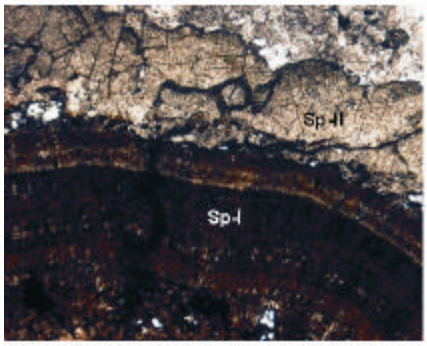

Figure 15e Colloform Sp-I rimmed by light yellow Sp-II as seen in transmitted light in doubly polished thin section (200 mm thick) sample P4-24. The base of the image corresponds to 1.3 mm.

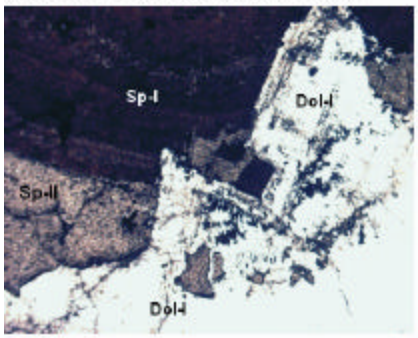

Figure 15g Colloform Sp-I, and Sp-II are brecciated by hydrothermal dolomite (Dol-I). Doubly polished thin section (200 mm thick) sample P4-24. Base of image corresponds to 2.6 mm.

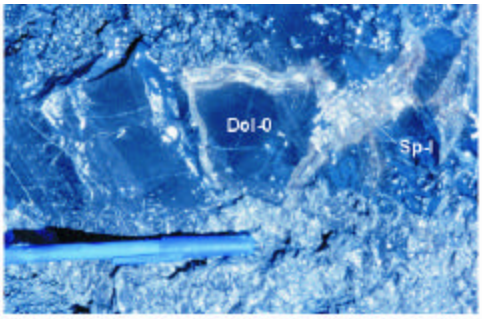

Figure 15b Rims of dark-brown coloured colloform Sp-I, generated by B-1 brecciation, around host dolomite fragments (Dol-0). Image from opencast pit. Rubble from mine-workings surround the area of focus.

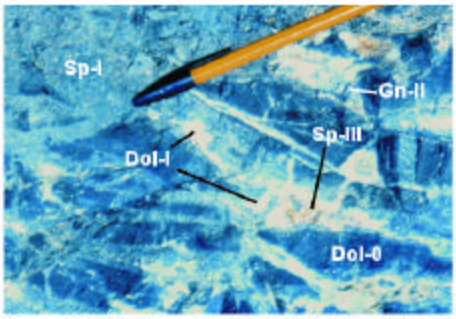

Figure 15d The brecciated dolomite host rock (Dol-0) is cemented by white hydrothermal dolomite (Dol-I) related to B-1. These fragments are coated and partly replaced by Sp-I, which clearly crosscuts B-1 brecciation. Yellow Sp-III and Gn-II precipitate in vugs created by subsequent brecciation events (B-2 and B-3).

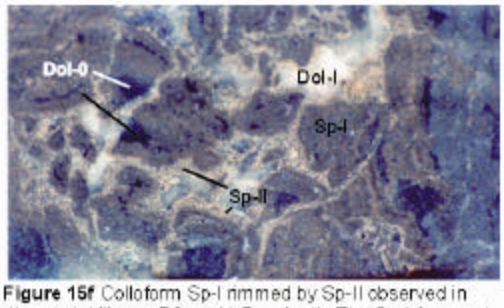

Figure 15f Colloform Sp-I rimmed by Sp-II observed in diamond drill core P2, at 41.7 m depth. The Sp-I fragments are rimmed by Sp-II, and then cemented by hydrothermal dolomite (Dol-I). The vertical dimension of the image is 4 cm.

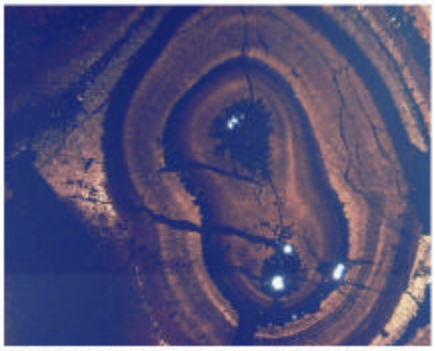

Figure 15h Concentric zoning of colloform Sp-I observed in doubly polished thin section P899-9B (200 mm thick). The radiating texture may be achieved by minute crystals projecting into a super-saturated ore-fluid. The varying colour bands and growth zones are attributed to varying physico-chemical environments of mineralisation through time. The base of image corresponds to 2.6 mm.

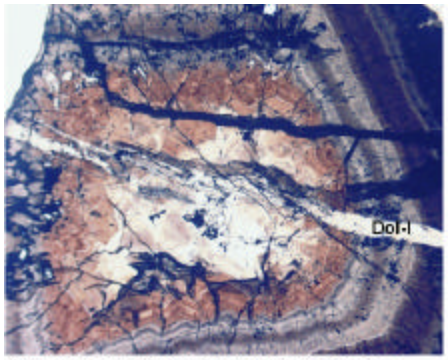

Figure 16a Concentric zoning in Sp-I in doubly polished thin section P899-9B (200 mm), viewed in transmitted light. Veins of hydrothermal dolomite (Dol-I) crosscut sphalerite mineralisation. Base of image equals 2.6 mm.

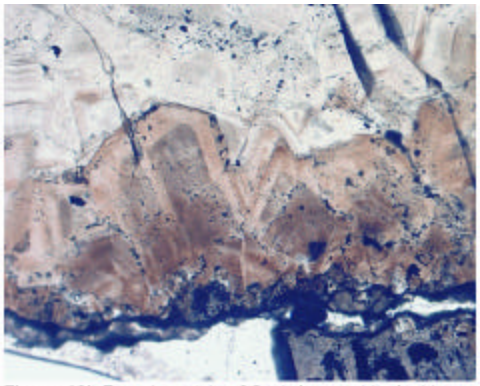

Figure 16b Zoned crystals of Sp-I observed in doubly polished thin section (200 mm) of sample P899-9B. This texture is indicative of the unobstructed growth of sphalerite into fluid-filled vugs. The banding may be due to changes in physico-chemical conditions during mineralisation. The base of the image corresponds to 1.3 mm.

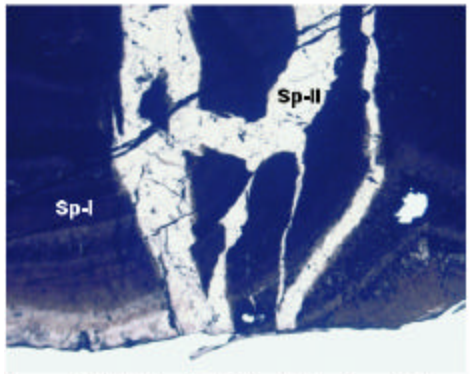

Figure 16c Colloform Sp-I infiltrated by veins of light yellow Sp-II observed in doubly polished thin section (200 mm thick) viewed in transmitted light (P899-9B). Base of image corresponds to 2.6 mm.

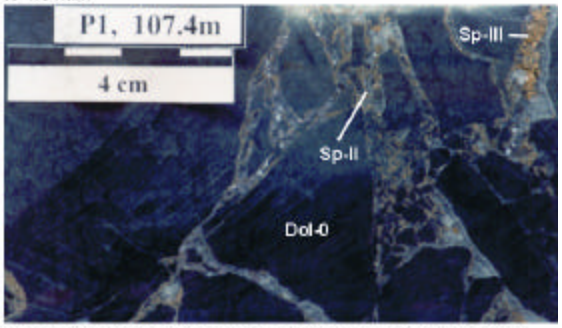

Figure 16d Yellow Sp-II occurring as rims around dolomite host (Dol-0) fragments, which have been brecciated by B-2. The Sp-II may occur contemporaneously with the infiltrating hydrothermal dolomite, or, alternatively, as early pre-existing precipitates rimming the dolomite host rock, which is subsequently brecciated by B-3 and cemented by hydrothermal dolomite. Sp-III is present as late-stage infil.

Figure 16e Brown coloured Sp-III occurring as open-space infil in the dolomite host (Dol-0), together with saddle-shaped hydrothermal dolomite crystals (Dol-I).

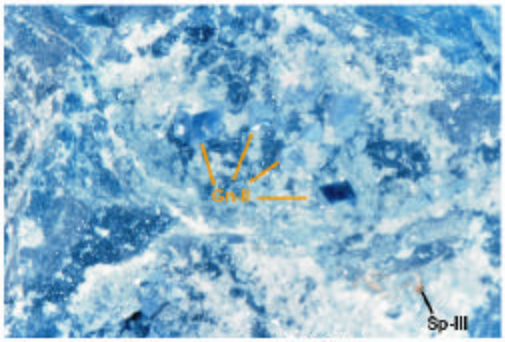

Figure 16f Euhedral galena crystals (Gn-II) as open-space infil associated with euhedral crystals of hydrothermal dolomite, Sp-III and calcite. The dolomite host is fragmented by dissolution, and cemented by hydrothermal dolomite. Base of the image equals 15 cm.

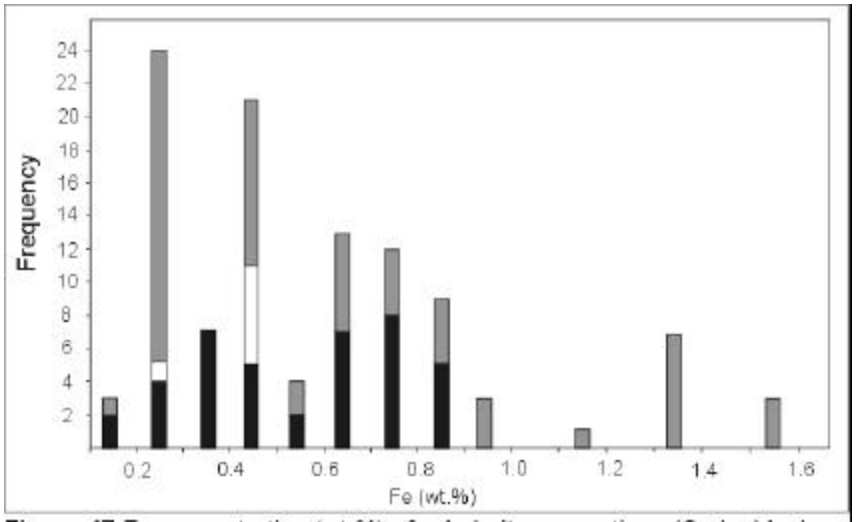

Figure 17 Fe concentration (wt.%) of sphalerite generations (Sp-I = black, Sp-II = white, Sp-III = grey).

confirmed with Raman microprobe analyses (Pasteris and Wopenka, 1991). Concentrations of other trace elements, including Ni, Co, Cd, As, Cu and Au were always below the detection limit of the electron microprobe.

Sphalerite II (Sp-II)

Sp-II is the least common ore mineral and occurs only as thin, transparent, yellow-coloured rims around Sp-I aggregates and host rock dolomite (Figs. 15e and 16d). Sp-II also forms network-like veins that crosscut fragments of Sp-I and the dolomite host rock, and is the product of brecciation event B-2. It predates the B-3 brecciation event and precipitation of sparry dolomite, Sp-III, Gn-II (Fig. 14 g,h), and forms contemporaneously with quartz (Fig. 14 g,h). The chemical composition of Sp-II is similar to that of Sp-I (Fig. 17).

Sphalerite III (Sp-III)

This final sphalerite generation is present as large, euhedral crystals (from a few mm to ~3 cm), closely associated with Dol-I, Gn-II and quartz as open-space infill in breccia bodies associated with the main brecciation event (B-3) (Figs. 15c, 16d,e). It has a yellow- to brown-honey colour in hand-specimen, and is weakly yellow-transparent in transmitted light. Some Sp-III grains show yellow luminescence. The chemical composition of Sp-III is similar to that of Sp-I and Sp-II (Fig. 17).

Galena I (Gn-I)

Gn-I occurs as fine-grained euhedral to anhedral grains finely intergrown with Sp-I in the early, disseminated mineralisation. Although galena is far less dominant than sphalerite in occurrence, some areas of predominantly disseminated Gn-I mineralisation are present (Terblanche, pers. comm., 1998). Gn-I appears to infiltrate the host dolomite, forming vein-like textures, which suggests an epigenetic origin for the mineralisation.

Galena II (Gn-II)

Large galena cubes are present as open-space infill associated with Sp-III, sparry dolomite and quartz. Crystals range in size from a few millimetres to three cm (Fig. 16f). It is volumetrically less dominant than Gn-I. Both generations of galena have a very simple chemical composition, without any detectable trace-element concentrations.

CONCLUSIONS

MVT deposits originate when metalliferous basinal brines migrate to sites suitable for the precipitation of zinc- and lead- sulphides. The metals in these brines may either be transported as chloride, reduced sulphur, or organic complexes. Mineralisation is caused by: (1) the mixing of the metal-chloride aqueous fluid with an external sulphur source at the site of mineralisation; (2) the reduction of sulphate by methane and/or organic material when metals are carried in a sulphate-chloride-bearing brine; or (3) the destabilisation of the carrier organic complexes in sulphurous fluids where metals are transported as organic and chloride complexes.

The Pering Pb-Zn deposit is known as one of the oldest MVT deposits. Three discernable sphalerite generations, with two galena generations, are hosted in the carbonate platform sequence of the Campbellrand Subgroup. Early ore mineral assemblages are brecciated and cemented by sparry dolomite and calcite, with subsequent ore assemblages, sparry dolomite, quartz and calcite filling in the open spaces created by dissolution and brecciation of the host.

ACKNOWLEDGEMENTS

This review formed part of an M.Sc. thesis completed at the Department of Geology, Rand Afrikaans University, Johannesburg. Funding was provided by the Department of Geology, RAU, Billiton SA Limited, the National Research Foundation of South Africa, and the Jim and Gladys Taylor Education Trust. In addition, N.J. Beukes, H.E. Frimmel, M. Boni, B.S.A. Wiggett, and the staff at Pering Mine are thanked for their help.

REFERENCES

Adams, A. E., MacKenzie, W. S. and Guilford, C. (1984). *Atlas of Sedimentary Rocks under the Microscope*. John Wiley and Sons, New York, 104pp.

Altermann, W. and Wotherspoon, J. McD. (1995). The carbonates of the Transvaal and Griqualand West Sequences of the Kaapvaal Craton, with special reference to the Lime Acres limestone deposit. *Mineralium Depositia,* **30**, 124 -134.

Anderson, G. M. (1991). Organic maturation and ore precipitation in southeast Missouri. *Economic Geology*, **86**, 909-926.

Barnes, H.L. (1979). Solubilities of ore minerals. *In*: Barnes H.L. (ed.), *Geochemistry of Hydrothermal Ore Deposits*, John Wiley and Sons, New York, p. 404-460.

Barrett, T. J. and Anderson, G. M. (1988). The solubility of sphalerite and galena in 1-5m NaCl solutions to 300 °C. *Geochimica et Cosmochimica Acta* , **52**, p. 813-820.

Barton, E.S., Altermann, W., Williams, I.S. and Smith, C.B. (1994). U-Pb zircon age for a tuff in the Campbellrand Group, Griqualand West Sequence, South Africa: implications for Early Proterozoic rock accumulation rates. *Geology*, **22**, 343-346.

Bathurst, R.G.C. (1975). *Carbonate Sediments and their Diagenesis.* (2nd ed.), *Developments in Sedimentology*, Elsevier, Amsterdam, **12**, 658 pp.

Beukes, N.J. (1978). *Die karbonaatgesteentes en ysterformasies van die Transvaal Supergroep in Noord-Kaapland.* Unpublished Ph.D. thesis, Rand Afrikaans University, Johannesburg, 580 pp.

Beukes, N.J. (1980). Lithofacies and stratigraphy of the Kuruman and Griquatown iron formations, Northern Cape Province, South Africa. *Transactions Geological Society South Africa*, **83**, 69-86.

Beukes, N.J. (1983). Paleoenvironmental setting of iron-formations in the depositional basin of the Transvaal Supergroup, South Africa. *In*: Trendall, A.F. and Morris, R. C. (eds.), *Iron Formations, Facts and Problems.* Elsevier, Amsterdam, p. 131-209.

Beukes, N.J. (1986). The Transvaal Sequence in Griqualand West. In: Anhaeusser, C.R. and Maske, S. (eds.), *Mineral Deposits of Southern Africa,* Volume I, The Geological Society of South Africa, Johannesburg, p. 819-828.

Beukes, N.J. (1987). Facies relations, depositional environments and diagenesis in a major early Proterozoic stromatolitic carbonate platform to basinal sequence, Campbellrand Subgroup, Transvaal Supergroup, southern Africa. *Sedimentary Geology*, **54**, 1-46.

Beukes, N.J., Klein, C., Kaufman, A.J. and Hayes, J.M. (1990). Carbonate petrography, kerogen distribution, and carbon and oxygen isotope variations in an Early Proterozoic transition from limestone to iron-formation deposition, Transvaal Supergroup, South Africa. *Economic Geology*, **85**, 663-690.

Button, A. (1973). The stratigraphic history of the Malmani Dolomite in the eastern and north-eastern Transvaal. *Transactions of the Geological Society of South Africa*, **76**, (3), 229-247.

Cathles, L.M. and Smith, A.T. (1983). Thermal constraints on the formation of Mississippi Valley-Type lead-zinc deposits and their implications for episodic basin dewatering and deposit genesis. *Economic Geology*, **78**, 983-1002.

Chi, G. and Savard, M. M. (1997). Sources of basinal and Mississippi Valley-Type mineralizing brines: mixing of evaporated seawater and halite-dissolution brine. *Chemical Geology*, **143**, 121-125.

Craig, J.R. and Vaughan, D.J. (1994). *Ore Microscopy and Ore Petrography.* 2nd ed., John Wiley and Sons, Singapore, 434 p.

Duane, M.J. and Saggerson, E.P. (1995). Brine expulsion, fluid transport and metallization spanning 2.0 Gyr in basins of southern and central Africa. *Basin Research*, **7**, 97-108.

Eriksson, K.A. and Truswell, J.F. (1974). Tidal flat associations from a lower Proterozoic carbonate sequence in South Africa. *Sedimentology*, **21**, 293-310.

Eriksson, P.G., Hattingh, P.J., Altermann, W. (1995). An overview of the geology of the Transvaal Sequence and Bushveld Complex, South Africa. *Mineralium Deposita*, **30**, 98-111.

Evans, D.A.D., Beukes, N.J., Kirschvink, J.L., (in press). Paleomagnetism of a lateritic paleo-weathering horizon and overlying Palaeoproterozoic red beds from the Kaapvaal Craton,

South Africa: a constraint on early Proterozoic atmospheric oxygen. Journal of Geophysical Research.

Folk, R.L. (1959). Practical petrographic classification of limestones. *Bulletin of American Associated Petroleum Geologists*, **43**, 1-38.

Giordano, T.H. and Barnes, H.L. (1979). Ore solution chemistry VI. PbS solubility in bisulphide solutions to 300 °C. *Economic Geology*, **74**, 1637-1646.

Giordano, T.H. and Barnes, H.L. (1981). Lead transport in Mississippi Valley-Type ore solutions. *Economic Geology*, **76**, 2200-2211.

Greyling, L.N. (2000). *The Paleoproterozoic carbonate-hosted Pering lead-zinc deposit, South Africa.* Unpublished M.Sc thesis, Rand Afrikaans University, Johannesburg, 129 pp.

Guilbert, J. M. and Park, C.F. (1986). *The Geology of Ore Deposits.* Freeman and Company, New York, 985 pp.

Gutzmer, J. (1996). *Genesis and alteration of the Kalahari and Postmasburg manganese deposits, Griqualand West, South Africa.* Unpublished Ph.D thesis, Rand Afrikaans University, 266 pp.

Heyl, A., Landis, G.P. and Zartman R.E. (1974). Isotopic evidence for the origin of Mississippi Valley-Type mineral deposits: review. *Economic Geology*, **69**, 992-1006.

Holland, T.J.B. and Powell, R. (1998). An internally consistent thermodynamic data set for phases of petrological interest. *Journal of Metamorphic Geology*, **16**, 309-343.

Klein, C. and Beukes, N.J. (1989). Geochemistry and sedimentology of a facies transition from limestone to iron-formation deposition in the Early Proterozoic Transvaal Supergroup, South Africa. *Economic Geology*, **84**, 1733-1774.

Kruger, F.J., Duane, M.J. and Whitelaw, H.T. (1999). The *c*.2 Ga Kheis tectonism in southern Africa and associated MVT mineralisation. *In*: Stanley et al. (eds.), *Mineral Deposits: Processes to Processing*, Rotterdam, p. 1263-1266.

Leach, D.L. and Sangster, D.F. (1993). Mississippi Valley-Type lead-zinc deposits. *In*: Kirkham, R.V., Sinclair, W.D., Thorpe, R.I. and Duke, J.M. (eds.), *Mineral Deposit Modelling*. Geological Association of Canada, Special Paper, **40**, 289-314.

Leighton, M.W. and Pendexter, C. (1962). Carbonate rock types. *In*: Ham, W. E. (eds.), Classification of carbonate rocks – a symposium. *The American Association of Petroleum Geologists, U S A, Memoir* **1**, p. 33-61.

Machel, H.G. and Burton, E.A. (1991). Factors governing cathodoluminescence in calcite and dolomite, and their implications for studies of carbonate diagenesis. *In*: Barker, C.E. and Kopp, D.C. (eds.), *Luminescence Microscopy: Quantitative and Qualitative Aspects.* SEPM Short Course **25**, p. 37-57.

Martini, J.E.J. (1986). The Zeerust fluorspar deposits, Western Transvaal. *In*: Anhaeusser, C.R. and Maske, S. (eds.), *Mineral Deposits of Southern Africa*, Volume I, The Geological Society of South Africa, Johannesburg, p. 837-841.

Martini, J.E.J., Eriksson, P.G. and Snyman, C.P. (1995). The early Proterozoic Mississippi Valley-Type Pb-Zn deposits of the Campbellrand and Malmani Subgroups, South Africa. *Mineralium Depositia,* **30**, 135-145.

Ohle, E.L. (1959). Some considerations in determining the origin of ore deposits of the Mississippi Valley-type. *Economic Geology,* **54**, 769-789.

Ohle, E.L. (1980). Some considerations in determining the origin of ore deposits of the Mississippi Valley-type – Part II. *Economic Geology,* **75**, 161-172.

Ohmoto, H. and Lasaga, A.C. (1982). Kinetics of reactions between aqueous sulfates and sulfides in hydrothermal systems. *Geochimica Cosmochimica Acta* , **46**, 1727-1745.

Orr, W. L. (1974). Changes in sulfur content and isotope ratios of sulfur during petroleum maturation – study of Big Horn Basin Paleozoic oils. *American Association of Petroleum Geology Bulletin*, **58**, 2295-2318.

Orr, W. L. (1982). Rate and mechanism of non-microbial sulfate reduction. *Geological Society of America, Abstract with Programs,* **14**, p. 580.

Pasteris, J.D. and Wopenka , B. (1991). Raman spectra of graphite as indicators of degree of metamorphism. *Canadian Mineralogist*, **29**, 1-9.

Pearson, R.G. (1963). Hard and soft acids and bases. *Journal of the American Chemical Society*, **45**, 581-587.

Roberts, P.J. (1992). *The geology and geochemistry of selected Pb-Zn deposits in the Chuniespoort/Ghaap Group of the Transvaal Sequence, South Africa.* Unpublished M.Sc. thesis, University of the Witwatersrand, Johannesburg, 192 pp.

Roberts, P.J., Gize, A.P., Duane, M.J. and Verhagen, B.T. (1993). Precambrian hydrocarbon residues associated with Mississippi Valley-Type mineralization in the Transvaal Sequence, South Africa. South African Journal of Geology, **96** (1/2), 57-60.

Rollinson, H.R. (1993). *Using Geochemical Data: Evaluation, Presentation, Interpretation.* Longman Geochemistry Series, Singapore, 352 pp.

Roedder, E. (1984). Fluid inclusions. *Mineralogical Society of America, Reviews in Mineralogy,* **12**, 646 pp.

SACS (South African Committee for Stratigraphy) (1980). Stratigraphy of South Africa, Part 1. (Comp. Kent, L.E.), Lithostratigraphy of the Republic of South Africa, South West Africa/Namibia and the Republics of Bophuthatswana, Transkei and Venda, *Handbook of the Geological Survey of South Africa,* 690 pp.

Schoonen, M.A.A. and Barnes, H.L. (1997). Chemical and physical data for hydrothermal systems. *In*: Barnes, H.L. (ed.), *Geochemistry of Hydrothermal Ore Deposits* (3rd ed.), John Wiley and Sons, New York, p. 937-962.

Seward, T.M. and Barnes, H.L. (1997). Metal transport by hydrothermal ore fluids. *In*: Barnes, H.L. (ed.), *Geochemistry of Hydrothermal Ore Deposits* (3rd ed.), John Wiley and Sons, New York, p. 435-486.

Sicree, A.A. and Barnes, H.L. (1996). Upper Mississippi Valley district ore fluid model: the role of organic complexes. *Ore Geology Reviews,* **11**, 105-131.

Skinner, B.J. (1997). Hydrothermal mineral deposits: what we do and don't know. *In*: Barnes, H.L. (ed.), *Geochemistry of Hydrothermal Ore Deposits* (3rd ed.), John Wiley and Sons, New York, p. 1-29.

Southwood, M.J. (1986). The mineralogy of the Pering zinc-lead deposit, Cape Province, with special reference to supergene alteration. *In*: Anhaeusser, C.R. and Maske, S. (eds.), *Mineral Deposits of Southern Africa*, Volume I, The Geological Society of South Africa, Johannesburg, p. 875-889.

Spirakes, C.S. and Heyl, A.V. (1995). Evaluation of proposed precipitation mechanisms for Mississippi Valley-Type deposits. *Ore Geology Reviews,* **10**, 1-17.

SSAM (Shell South Africa Metals Division) (1988). Pering Mine geology. *Geobulletin*, The Geological Society of South Africa, 2nd Quarter, **31** (2), p. 30-33.

Sumner, D.Y. and Bowring, S.A. (1996). U-Pb geochronologic constraints on deposition of the Campbellrand Subgroup, Transvaal Supergroup, South Africa. *Precambrian Research,* **79**, 25-35.

Sverjenski, D.A. (1981). The origin of a Mississippi Valley-Type deposit in the Viburnam trend, southeast Missouri. *Economic Geology*, **76**, 1848-1872.

Sverjenski, D.A. (1986). Genesis of Mississippi Valley-Type lead-zinc deposits. *Annual Reviews of Earth Planetary Sciences*, **14**, 177-199.

Tankard, A.J., Jackson, M.P.A., Eriksson, K.A., Hobday, D.K., Hunter, D.R. and Minter, W.E.L. (1982). *Crustal Evolution of Southern Africa.* Springer-Verlag, New York, 523 pp.

Trendall, A. et al. (1990). Precise zircon U-Pb chronological comparison of the volcano-sedimentary sequences of the Kaapvaal and Pilbara cratons between about 3.1 and 2.4 Ga. *Extended Abstract, Third International Archaean Symposium, Perth, Australia,* p. 81-83.

Turner, A. M. (1992*). Zinc-lead mineralization at Pering Mine in the Griqualand West sub-basin – an isotopic study.* Unpublished M.Sc. thesis, University of Natal, Durban, 90 pp.

Wheatley, C.J.V., Whitfield, G.G., Kenny, K.J. and Birch, A. (1986). The Pering carbonate-hosted zinc-lead deposit, Griqualand West. *In*: Anhaeusser, C.R. and Maske, S. (eds.), *Mineral Deposits of Southern Africa,* Volume I, The Geological Society of South Africa, Johannesburg, p. 867-874.

Wood, S.A. and Samson, I.M. (1998). Solubility of ore minerals and complexation of ore metals in hydrothermal solutions. *In*: Richards, J.P. and Larson, P.B. (eds.), Techniques in hydrothermal ore deposits geology. *Society of Economic Geologists Inc*., *Reviews in Economic Geology*, **10**, p. 33-80.

_____oOo_____